

See discussions, stats, and author profiles for this publication at: <https://www.researchgate.net/publication/2995027>

# On the Use of Windows for Harmonic Analysis With the Discrete Fourier Transform

Article in *Proceedings of the IEEE* · February 1978

DOI: 10.1109/PROC.1978.10837 · Source: IEEE Xplore

CITATIONS

6,644

READS

10,651

1 author:



[fred joel harris](#)

San Diego State University

193 PUBLICATIONS 9,019 CITATIONS

SEE PROFILE

Some of the authors of this publication are also working on these related projects:



Multirate Signal Processing for SDR and CR [View project](#)

# On the Use of Windows for Harmonic Analysis with the Discrete Fourier Transform

FREDRIC J. HARRIS, MEMBER, IEEE

**Abstract**—This paper makes available a concise review of data windows and their affect on the detection of harmonic signals in the presence of broad-band noise, and in the presence of nearby strong harmonic interference. We also call attention to a number of common errors in the application of windows when used with the fast Fourier transform. This paper includes a comprehensive catalog of data windows along with their significant performance parameters from which the different windows can be compared. Finally, an example demonstrates the use and value of windows to resolve closely spaced harmonic signals characterized by large differences in amplitude.

## I. INTRODUCTION

THERE IS MUCH signal processing devoted to detection and estimation. Detection is the task of determining if a specific signal set is present in an observation, while estimation is the task of obtaining the values of the parameters describing the signal. Often the signal is complicated or is corrupted by interfering signals or noise. To facilitate the detection and estimation of signal sets, the observation is decomposed by a basis set which spans the signal space [1]. For many problems of engineering interest, the class of signals being sought are periodic which leads quite naturally to a decomposition by a basis consisting of simple periodic functions, the sines and cosines. The classic Fourier transform is the mechanism by which we are able to perform this decomposition.

By necessity, every observed signal we process must be of finite extent. The extent may be adjustable and selectable, but it must be finite. Processing a finite-duration observation imposes interesting and interacting considerations on the harmonic analysis. These considerations include detectability of tones in the presence of nearby strong tones, resolvability of similar-strength nearby tones, resolvability of shifting tones, and biases in estimating the parameters of any of the aforementioned signals.

For practicality, the data we process are  $N$  uniformly spaced samples of the observed signal. For convenience,  $N$  is highly composite, and we will assume  $N$  is even. The harmonic estimates we obtain through the discrete Fourier transform (DFT) are  $N$  uniformly spaced samples of the associated periodic spectra. This approach is elegant and attractive when the processing scheme is cast as a spectral decomposition in an  $N$ -dimensional orthogonal vector space [2]. Unfortunately, in many practical situations, to obtain meaningful results this elegance must be compromised. One such

compromise consists of applying windows to the sampled data set, or equivalently, smoothing the spectral samples.

The two operations to which we subject the data are sampling and windowing. These operations can be performed in either order. Sampling is well understood, windowing is less so, and sampled windows for DFT's significantly less so! We will address the interacting considerations of window selection in harmonic analysis and examine the special considerations related to sampled windows for DFT's.

## II. HARMONIC ANALYSIS OF FINITE-EXTENT DATA AND THE DFT

Harmonic analysis of finite-extent data entails the projection of the observed signal on a basis set spanning the observation interval [1], [3]. Anticipating the next paragraph, we define  $T$  seconds as a convenient time interval and  $NT$  seconds as the observation interval. The sines and cosines with periods equal to an integer submultiple of  $NT$  seconds form an orthogonal basis set for continuous signals extending over  $NT$  seconds. These are defined as

$$\left. \begin{aligned} \cos \left[ \frac{2\pi}{NT} kt \right] \\ \sin \left[ \frac{2\pi}{NT} kt \right] \end{aligned} \right\} \quad \begin{aligned} k = 0, 1, \dots, N-1, N, N+1, \dots \\ 0 \leq t < NT. \end{aligned} \quad (1)$$

We observe that by defining a basis set over an ordered index  $k$ , we are defining the spectrum over a line (called the frequency axis) from which we draw the concepts of bandwidth and of frequencies close to and far from a given frequency (which is related to resolution).

For sampled signals, the basis set spanning the interval of  $NT$  seconds is identical with the sequences obtained by uniform samples of the corresponding continuous spanning set up to the index  $N/2$ ,

$$\left. \begin{aligned} \cos \left[ \frac{2\pi}{NT} knT \right] = \cos \left[ \frac{2\pi}{N} kn \right] \\ \sin \left[ \frac{2\pi}{NT} knT \right] = \sin \left[ \frac{2\pi}{N} kn \right] \end{aligned} \right\} \quad \begin{aligned} k = 0, 1, \dots, N/2 \\ n = 0, 1, \dots, N-1. \end{aligned} \quad (2)$$

We note here that the trigonometric functions are unique in that uniformly spaced samples (over an integer number of periods) form orthogonal sequences. Arbitrary orthogonal functions, similarly sampled, do not form orthogonal sequences. We also note that an interval of length  $NT$  seconds is not the same as the interval covered by  $N$  samples separated by intervals of  $T$  seconds. This is easily understood when we

Manuscript received September 10, 1976; revised April 11, 1977 and September 1, 1977. This work was supported by Naval Undersea Center (now Naval Ocean Systems Center) Independent Exploratory Development Funds.

The author is with the Naval Ocean Systems Center, San Diego, CA, and the Department of Electrical Engineering, School of Engineering, San Diego State University, San Diego, CA 92182.

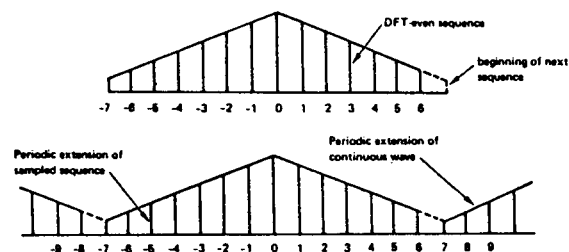

 Fig. 1.  $N$  samples of an even function taken over an  $NT$  second interval.


Fig. 2. Even sequence under DFT and periodic extension of sequence under DFT.

realize that the interval over which the samples are taken is closed on the left and is open on the right (i.e.,  $[-, )$ ). Fig. 1 demonstrates this by sampling a function which is even about its midpoint and of duration  $NT$  seconds.

Since the DFT essentially considers sequences to be periodic, we can consider the missing end point to be the beginning of the next period of the periodic extension of this sequence. In fact, under the periodic extension, the next sample (at 16 s in Fig. 1.) is indistinguishable from the sample at zero seconds.

This apparent lack of symmetry due to the missing (but implied) end point is a source of confusion in sampled window design. This can be traced to the early work related to convergence factors for the partial sums of the Fourier series. The partial sums (or the finite Fourier transform) always include an odd number of points and exhibit even symmetry about the origin. Hence much of the literature and many software libraries incorporate windows designed with true even symmetry rather than the implied symmetry with the missing end point!

We must remember for DFT processing of sampled data that even symmetry means that the projection upon the sampled sine sequences is identically zero; it does not mean a matching left and right data point about the midpoint. To distinguish this symmetry from conventional evenness we will refer to it as DFT-even (i.e., a conventional even sequence with the right-end point removed). Another example of DFT-even symmetry is presented in Fig. 2 as samples of a periodically extended triangle wave.

If we evaluate a DFT-even sequence via a finite Fourier transform (by treating the  $+N/2$  point as a zero-value point), the resultant continuous periodic function exhibits a non zero imaginary component. The DFT of the same sequence is a set of samples of the finite Fourier transform, yet these samples exhibit an imaginary component equal to zero. Why the disparity? We must remember that the missing end point under the DFT symmetry contributes an imaginary sinusoidal component of period  $2\pi/(N/2)$  to the finite transform (corresponding to the odd component at sequence position  $N/2$ ). The sampling positions of the DFT are at the multiples of  $2\pi/N$ , which, of course, correspond to the zeros of the imaginary sinusoidal component. An example of this fortuitous sampling is shown in Fig. 3. Notice the sequence  $f(n)$ ,

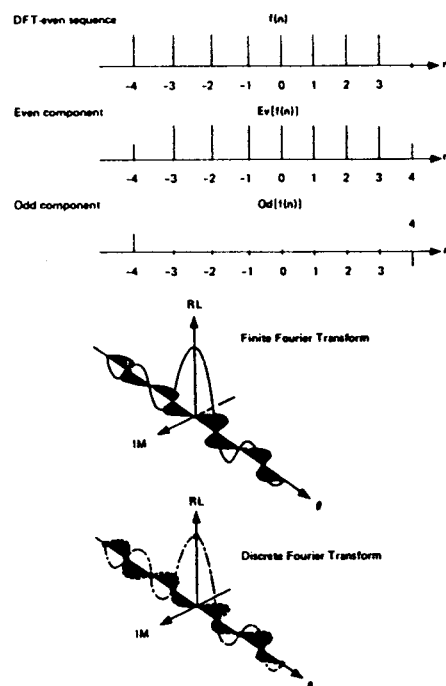


Fig. 3. DFT sampling of finite Fourier transform of a DFT even sequence.

is decomposed into its even and odd parts, with the odd part supplying the imaginary sine component in the finite transform.

### III. SPECTRAL LEAKAGE

The selection of a finite-time interval of  $NT$  seconds and of the orthogonal trigonometric basis (continuous or sampled) over this interval leads to an interesting peculiarity of the spectral expansion. From the continuum of possible frequencies, only those which coincide with the basis will project onto a single basis vector; all other frequencies will exhibit non zero projections on the entire basis set. This is often referred to as spectral leakage and is the result of processing finite-duration records. Although the amount of leakage is influenced by the sampling period, leakage is not caused by the sampling.

An intuitive approach to leakage is the understanding that signals with frequencies other than those of the basis set are not periodic in the observation window. The periodic extension of a signal not commensurate with its natural period exhibits discontinuities at the boundaries of the observation. The discontinuities are responsible for spectral contributions (or leakage) over the entire basis set. The forms of this discontinuity are demonstrated in Fig. 4.

Windows are weighting functions applied to data to reduce the spectral leakage associated with finite observation intervals. From one viewpoint, the window is applied to data (as a multiplicative weighting) to reduce the order of the discontinuity at the boundary of the periodic extension. This is accomplished by matching as many orders of derivative (of the weighted data) as possible at the boundary. The easiest way to achieve this matching is by setting the value of these derivatives to zero or near to zero. Thus windowed data are smoothly brought to zero at the boundaries so that the periodic extension of the data is continuous in many orders of derivative.

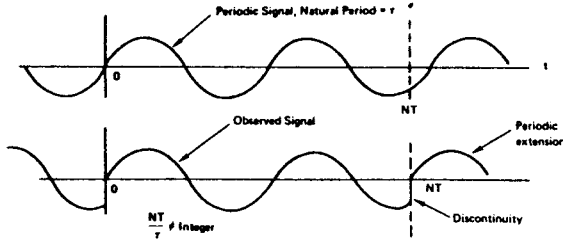


Fig. 4. Periodic extension of sinusoid not periodic in observation interval.

From another viewpoint, the window is multiplicatively applied to the basis set so that a signal of arbitrary frequency will exhibit a significant projection only on those basis vectors having a frequency close to the signal frequency. Of course both viewpoints lead to identical results. We can gain insight into window design by occasionally switching between these viewpoints.

#### IV. WINDOWS AND FIGURES OF MERIT

Windows are used in harmonic analysis to reduce the undesirable effects related to spectral leakage. Windows impact on many attributes of a harmonic processor; these include detectability, resolution, dynamic range, confidence, and ease of implementation. We would like to identify the major parameters that will allow performance comparisons between different windows. We can best identify these parameters by examining the effects on harmonic analysis of a window.

An essentially bandlimited signal  $f(t)$  with Fourier transform  $F(\omega)$  can be described by the uniformly sampled data set  $f(nT)$ . This data set defines the periodically extended spectrum  $F^T(\omega)$  by its Fourier series expansion as identified as

$$F(\omega) = \int_{-\infty}^{+\infty} f(t) \exp(-j\omega t) dt \quad (3a)$$

$$F^T(\omega) = \sum_{n=-\infty}^{+\infty} f(nT) \exp(-j\omega nT) \quad (3b)$$

$$f(t) = \int_{-\pi/T}^{+\pi/T} F^T(\omega) \exp(+j\omega t) d\omega/2\pi \quad (3c)$$

$$|F(\omega)| = 0, \quad |\omega| \geq \frac{1}{2} [2\pi/T]$$

and where

$$F^T(\omega) = F(\omega), \quad |\omega| \leq \frac{1}{2} [2\pi/T].$$

For (real-world) machine processing, the data must be of finite extent, and the summation of (3b) can only be performed as a finite approximation as indicated as

$$F_a(\omega) = \sum_{n=-N/2}^{+N/2} f(nT) \exp(-j\omega nT), \quad N \text{ even} \quad (4a)$$

$$F_b(\omega) = \sum_{n=-N/2}^{(N/2)-1} f(nT) \exp(-j\omega nT), \quad N \text{ even} \quad (4b)$$

$$F_c(\omega_k) = \sum_{n=-N/2}^{(N/2)-1} f(nT) \exp(-j\omega_k nT), \quad N \text{ even} \quad (4c)$$

$$F_d(\omega_k) = \sum_{n=0}^{N-1} f(nT) \exp(-j\omega_k nT), \quad N \text{ even} \quad (4d)$$

where

$$\omega_k = \frac{2\pi}{NT} k, \quad \text{and } k = 0, 1, \dots, N-1.$$

We recognize (4a) as the finite Fourier transform, a summation addressed for the convenience of its even symmetry. Equation (4b) is the finite Fourier transform with the right-end point deleted, and (4c) is the DFT sampling of (4b). Of course for actual processing, we desire (for counting purposes in algorithms) that the index start at zero. We accomplish this by shifting the starting point of the data  $N/2$  positions, changing (4c) to (4d). Equation (4d) is the forward DFT. The  $N/2$  shift will affect only the phase angles of the transform, so for the convenience of symmetry we will address the windows as being centered at the origin. We also identify this convenience as a major source of window misapplication. The shift of  $N/2$  points and its resultant phase shift is often overlooked or is improperly handled in the definition of the window when used with the DFT. This is particularly so when the windowing is performed as a spectral convolution. See the discussion on the Hanning window under the  $\cos^2(X)$  windows.

The question now posed is, to what extent is the finite summation of (4b) a meaningful approximation of the infinite summation of (3b)? In fact, we address the question for a more general case of an arbitrary window applied to the time function (or series) as presented in

$$F_w(\omega) = \sum_{n=-\infty}^{+\infty} w(nT) f(nT) \exp(-j\omega nT) \quad (5)$$

where

$$w(nT) = 0, \quad |n| > \frac{N}{2}, \quad N \text{ even}$$

and

$$w(nT) = w(-nT), \quad n \neq \frac{N}{2}, \quad w\left(\frac{N}{2}T\right) = 0.$$

Let us now examine the effects of the window on our spectral estimates. Equation (5) shows that the transform  $F_w(\omega)$  is the transform of a product. As indicated in the following equation, this is equivalent to the convolution of the two corresponding transforms (see Appendix):

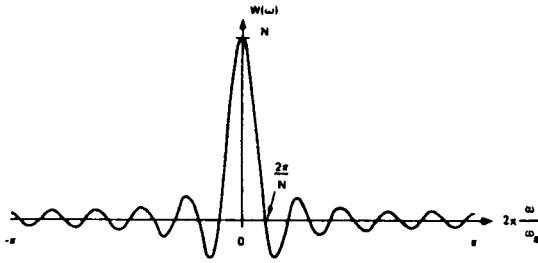
$$F_w(\omega) = \int_{-\infty}^{+\infty} F(x) W(\omega - x) dx/2\pi \quad (6)$$

or

$$F_w(\omega) = F(\omega) * W(\omega).$$

Equation (6) is the key to the effects of processing finite-extent data. The equation can be interpreted in two equivalent ways, which will be more easily visualized with the aid of an example. The example we choose is the sampled rectangle window;  $w(nT) = 1.0$ . We know  $W(\omega)$  is the Dirichlet kernel [4] presented as

$$W(\omega) = \exp\left(+j\frac{\omega T}{2}\right) \frac{\sin\left[\frac{N}{2}\omega T\right]}{\sin\left[\frac{1}{2}\omega T\right]}. \quad (7)$$


 Fig. 5. Dirichlet kernel for  $N$  point sequence.

Except for the linear phase shift term (which will change due to the  $N/2$  point shift for realizability), a single period of the transform has the form indicated in Fig. 5. The observation concerning (6) is that the value of  $F_w(\omega)$  at a particular  $\omega$ , say  $\omega = \omega_0$ , is the sum of all of the spectral contributions at each  $\omega$  weighted by the window centered at  $\omega_0$  and measured at  $\omega$  (see Fig. 6).

#### A. Equivalent Noise Bandwidth

From Fig. 6, we observe that the amplitude of the harmonic estimate at a given frequency is biased by the accumulated broad-band noise included in the bandwidth of the window. In this sense, the window behaves as a filter, gathering contributions for its estimate over its bandwidth. For the harmonic detection problem, we desire to minimize this accumulated noise signal, and we accomplish this with small-bandwidth windows. A convenient measure of this bandwidth is the equivalent noise bandwidth (ENBW) of the window. This is the width of a rectangle filter with the same peak power gain that would accumulate the same noise power (see Fig. 7).

The accumulated noise power of the window is defined as

$$\text{Noise Power} = N_0 \int_{-\pi/T}^{+\pi/T} |W(\omega)|^2 d\omega/2\pi \quad (8)$$

where  $N_0$  is the noise power per unit bandwidth. Parseval's theorem allows (8) to be computed by

$$\text{Noise Power} = \frac{N_0}{T} \sum_n w^2(nT). \quad (9)$$

The peak power gain of the window occurs at  $\omega = 0$ , the zero frequency power gain, and is defined by

$$\text{Peak Signal Gain} \doteq W(0) = \sum_n w(nT) \quad (10a)$$

$$\text{Peak Power Gain} = W^2(0) = \left[ \sum_n w(nT) \right]^2 \quad (10b)$$

Thus the ENBW (normalized by  $N_0/T$ , the noise power per bin) is given in the following equation and is tabulated for the windows of this report in Table I

$$\text{ENBW} = \frac{\sum_n w^2(nT)}{\left[ \sum_n w(nT) \right]^2}. \quad (11)$$

#### B. Processing Gain

A concept closely allied to ENBW is processing gain (PG) and processing loss (PL) of a windowed transform. We can think of the DFT as a bank of matched filters, where each

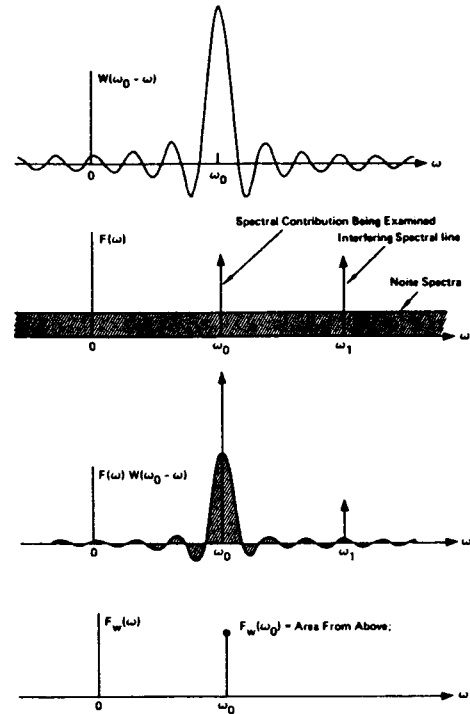


Fig. 6. Graphical interpretation of equation (6). Window visualized as a spectral filter.

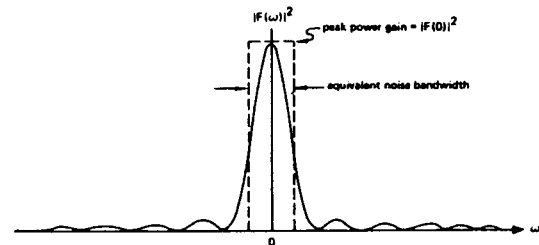


Fig. 7. Equivalent noise bandwidth of window.

filter is matched to one of the complex sinusoidal sequences of the basis set [3]. From this perspective, we can examine the PG (sometimes called the coherent gain) of the filter, and we can examine the PL due to the window having reduced the data to zero values near the boundaries. Let the input sampled sequence be defined by (12):

$$f(nT) = A \exp(+j\omega_k nT) + q(nT) \quad (12)$$

where  $q(nT)$  is a white-noise sequence with variance  $\sigma_q^2$ . Then the signal component of the windowed spectrum (the matched filter output) is presented in

$$\begin{aligned} F(\omega_k) |_{\text{signal}} &= \sum_n w(nT) A \exp(+j\omega_k nT) \exp(-j\omega_k nT) \\ &= A \sum_n w(nT). \end{aligned} \quad (13)$$

We see that the noiseless measurement (the expected value of the noisy measurement) is proportional to the input amplitude  $A$ . The proportionality factor is the sum of the window terms, which is in fact the dc signal gain of the window. For a rectangle window this factor is  $N$ , the number of terms in the window. For any other window, the gain is reduced due to the window smoothly going to zero near the boundaries. This

TABLE I  
WINDOWS AND FIGURES OF MERIT

WINDOW	HIGHEST SIDE- LOBE LEVEL (dB)	SIDE- LOBE FALL- OFF (dB/OCT)	COHERENT GAIN	EQUIV NOISE BW (BINS)	3.0-dB BW (BINS)	SCALLOP LOSS (dB)	WORST CASE PROCESS LOSS (dB)	6.0-dB BW (BINS)	OVERLAP CORRELATION (PCNT)	
									75% OL	50% OL
RECTANGLE	-13	-6	1.00	1.00	0.89	3.92	3.92	1.21	75.0	50.0
TRIANGLE	-27	-12	0.50	1.33	1.28	1.82	3.07	1.78	71.9	25.0
COS <sup>a</sup> (x) HANNING a = 1.0 a = 2.0 a = 3.0 a = 4.0	-23	-12	0.64	1.23	1.20	2.10	3.01	1.65	75.5	31.8
	-32	-18	0.50	1.50	1.44	1.42	3.18	2.00	65.9	16.7
	-39	-24	0.42	1.73	1.66	1.08	3.47	2.32	56.7	8.5
	-47	-30	0.38	1.94	1.86	0.86	3.75	2.59	48.6	4.3
HAMMING	-43	-6	0.54	1.36	1.30	1.78	3.10	1.81	70.7	23.5
RIESZ	-21	-12	0.67	1.20	1.16	2.22	3.01	1.59	76.5	34.4
RIEMANN	-26	-12	0.59	1.30	1.26	1.89	3.03	1.74	73.4	27.4
DE LA VALLE- POUSSIN	-53	-24	0.38	1.92	1.82	0.90	3.72	2.55	49.3	5.0
TUKEY a = 0.25 a = 0.50 a = 0.75	-14	-18	0.88	1.10	1.01	2.96	3.39	1.38	74.1	44.4
	-15	-18	0.75	1.22	1.15	2.24	3.11	1.57	72.7	36.4
	-19	-18	0.63	1.36	1.31	1.73	3.07	1.80	70.5	25.1
BOHMAN	-46	-24	0.41	1.79	1.71	1.02	3.54	2.38	54.5	7.4
POISSON a = 2.0 a = 3.0 a = 4.0	-19	-6	0.44	1.30	1.21	2.09	3.23	1.69	69.9	27.8
	-24	-6	0.32	1.65	1.45	1.46	3.64	2.08	54.8	15.1
	-31	-6	0.25	2.08	1.75	1.03	4.21	2.58	40.4	7.4
HANNING- POISSON a = 0.5 a = 1.0 a = 2.0	-35	-18	0.43	1.61	1.54	1.26	3.33	2.14	61.3	12.6
	-39	-18	0.38	1.73	1.64	1.11	3.50	2.30	56.0	9.2
	NONE	-18	0.29	2.02	1.87	0.87	3.94	2.65	44.6	4.7
CAUCHY a = 3.0 a = 4.0 a = 5.0	-31	-6	0.42	1.48	1.34	1.71	3.40	1.90	61.6	20.2
	-35	-6	0.33	1.76	1.50	1.36	3.83	2.20	48.8	13.2
	-30	-6	0.28	2.06	1.68	1.13	4.28	2.53	38.3	9.0
GAUSSIAN a = 2.5 a = 3.0 a = 3.5	-42	-6	0.51	1.39	1.33	1.69	3.14	1.86	67.7	20.0
	-55	-6	0.43	1.64	1.55	1.25	3.40	2.18	57.5	10.6
	-69	-6	0.37	1.90	1.79	0.94	3.73	2.52	47.2	4.9
DOLPH- CHEBYSHEV a = 2.5 a = 3.0 a = 3.5 a = 4.0	-50	0	0.53	1.39	1.33	1.70	3.12	1.85	69.6	22.3
	-60	0	0.48	1.51	1.44	1.44	3.23	2.01	64.7	16.3
	-70	0	0.45	1.62	1.55	1.25	3.35	2.17	60.2	11.9
	-80	0	0.42	1.73	1.65	1.10	3.48	2.31	55.9	8.7
KAISER- BESSEL a = 2.0 a = 2.5 a = 3.0 a = 3.5	-46	-6	0.49	1.50	1.43	1.46	3.20	1.99	65.7	16.9
	-57	-6	0.44	1.65	1.57	1.20	3.38	2.20	59.5	11.2
	-69	-6	0.40	1.80	1.71	1.02	3.56	2.39	53.9	7.4
	-82	-6	0.37	1.93	1.83	0.89	3.74	2.57	48.8	4.8
BARCILON- TEMES a = 3.0 a = 3.5 a = 4.0	-53	-6	0.47	1.56	1.49	1.34	3.27	2.07	63.0	14.2
	-58	-6	0.43	1.67	1.59	1.18	3.40	2.23	58.6	10.4
	-68	-6	0.41	1.77	1.69	1.05	3.52	2.36	54.4	7.6
EXACT BLACKMAN	-51	-6	0.46	1.57	1.52	1.33	3.29	2.13	62.7	14.0
BLACKMAN	-58	-18	0.42	1.73	1.68	1.10	3.47	2.35	56.7	9.0
MINIMUM 3-SAMPLE BLACKMAN-HARRIS	-67	-6	0.42	1.71	1.66	1.13	3.45	1.81	57.2	9.6
* MINIMUM 4-SAMPLE BLACKMAN-HARRIS	-92	-6	0.36	2.00	1.90	0.83	3.85	2.72	46.0	3.8
* 61 dB 3-SAMPLE BLACKMAN-HARRIS	-61	-6	0.45	1.61	1.56	1.27	3.34	2.19	61.0	12.6
74 dB 4-SAMPLE BLACKMAN-HARRIS	-74	-6	0.40	1.79	1.74	1.03	3.56	2.44	53.9	7.4
4-SAMPLE a = 3.0 KAISER-BESSEL	-69	-6	0.40	1.80	1.74	1.02	3.56	2.44	53.9	7.4

\*REFERENCE POINTS FOR DATA ON FIGURE 12 - NO FIGURES TO MATCH THESE WINDOWS.

reduction in proportionality factor is important as it represents a known bias on spectral amplitudes. Coherent power gain, the square of coherent gain, is occasionally the parameter listed in the literature. Coherent gain (the summation of (13)) normalized by its maximum value  $N$  is listed in Table I.

The incoherent component of the windowed transform is given by

$$F(\omega_k)|_{\text{noise}} = \sum_n w(nT) q(nT) \exp(-j\omega_k nT) \quad (14a)$$

and the incoherent power (the mean-square value of this component where  $E\{\cdot\}$  is the expectation operator) is given by

$$\begin{aligned} E\{|F(\omega_k)|_{\text{noise}}|^2\} &= \sum_n \sum_m w(nT) w(mT) E\{q(nT) q^*(mT)\} \\ &\quad \cdot \exp(-j\omega_k nT) \exp(+j\omega_k mT) \\ &= \sigma_q^2 \sum_n w^2(nT). \end{aligned} \quad (14b)$$

Notice the incoherent power gain is the sum of the squares of the window terms, and the coherent power gain is the square of the sum of the window terms.

Finally, PG, which is defined as the ratio of output signal-to-noise ratio to input signal-to-noise ratio, is given by

$$\begin{aligned} \text{PG} = \frac{S_o/N_o}{S_i/N_i} &= \frac{A^2 \left[ \sum_n w(nT) \right]^2 / \sigma_q^2 \sum_n w^2(nT)}{A^2 / \sigma_q^2} \\ &= \frac{\left[ \sum_n w(nT) \right]^2}{\sum_n w^2(nT)}. \end{aligned} \quad (15)$$

Notice PG is the reciprocal of the normalized ENBW. Thus large ENBW suggests a reduced processing gain. This is reasonable, since an increased noise bandwidth permits additional noise to contribute to a spectral estimate.

### C. Overlap Correlation

When the fast Fourier transform (FFT) is used to process long-time sequences a partition length  $N$  is first selected to establish the required spectral resolution of the analysis. Spectral resolution of the FFT is defined in (16) where  $\Delta f$  is the resolution,  $f_s$  is the sample frequency selected to satisfy the Nyquist criterion, and  $\beta$  is the coefficient reflecting the bandwidth increase due to the particular window selected. Note that  $[f_s/N]$  is the minimum resolution of the FFT which we denote as the FFT bin width. The coefficient  $\beta$  is usually selected to be the ENBW in bins as listed in Table I

$$\Delta f = \beta \left( \frac{f_s}{N} \right). \quad (16)$$

If the window and the FFT are applied to nonoverlapping partitions of the sequence, as shown in Fig. 8, a significant part of the series is ignored due to the window's exhibiting small values near the boundaries. For instance, if the transform is being used to detect short-duration tone-like signals, the non overlapped analysis could miss the event if it occurred near the boundaries. To avoid this loss of data, the transforms are usually applied to the overlapped partition sequences as shown in Fig. 8. The overlap is almost always 50 or 75 percent. This overlap processing of course increases the work load to cover the total sequence length, but the rewards warrant the extra effort.

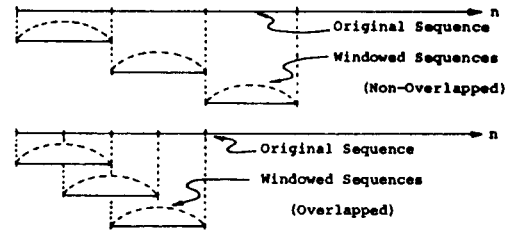


Fig. 8. Partition of sequences for nonoverlapped and for overlapped processing.

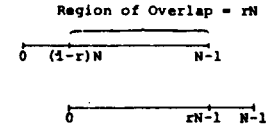


Fig. 9. Relationship between indices on overlapped intervals.

An important question related to overlapped processing is what is the degree of correlation of the random components in successive transforms? This correlation, as a function of fractional overlap  $r$ , is defined for a relatively flat noise spectrum over the window bandwidth by (17). Fig. 9 identifies how the indices of (17) relate to the overlap of the intervals. The correlation coefficient

$$c(r) = \frac{\left\{ \sum_{n=0}^{rN-1} (W(n) W(n + [1-r]N)) \right\}}{\left\{ \sum_{n=0}^{N-1} W^2(n) \right\}} \quad (17)$$

is computed and tabulated in Table I. for each of the windows listed for 50- and 75-percent overlap.

Often in a spectral analysis, the squared magnitude of successive transforms are averaged to reduce the variance of the measurements [5]. We know of course that when we average  $K$  identically distributed independent measurements, the variance of the average is related to the individual variance of the measurements by

$$\frac{\sigma_{\text{Avg.}}^2}{\sigma_{\text{Meas.}}^2} = \frac{1}{K}. \quad (18)$$

Now we can ask what is the reduction in the variance when we average measurements which are correlated as they are for overlapped transforms? Welch [5] has supplied an answer to this question which we present here, for the special case of 50- and 75-percent overlap

$$\frac{\sigma_{\text{Avg.}}^2}{\sigma_{\text{Meas.}}^2} = \frac{1}{K} [1 + 2c^2(0.5)] - \frac{2}{K^2} [c^2(0.5)],$$

50 percent overlap

$$\begin{aligned} &= \frac{1}{K} [1 + 2c^2(0.75) + 2c^2(0.5) + 2c^2(0.25)] \\ &\quad - \frac{2}{K^2} [c^2(0.75) + 2c^2(0.5) + 3c^2(0.25)], \end{aligned}$$

75 percent overlap. (19)

The negative terms in (19) are the edge effects of the average and can be ignored if the number of terms  $K$  is larger than ten. For good windows,  $c^2(0.25)$  is small compared to 1.0,

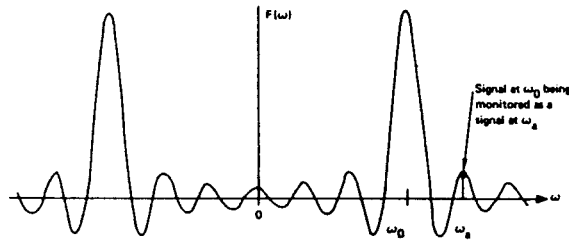


Fig. 10. Spectral leakage effect of window.

and can also be omitted from (19) with negligible error. For this reason,  $c(0.25)$  was not listed in Table I. Note, that for good windows (see last paragraph of Section IV-F), transforms taken with 50-percent overlap are essentially independent.

#### D. Scalping Loss

An important consideration related to minimum detectable signal is called scalping loss or picket-fence effect. We have considered the windowed DFT as a bank of matched filters and have examined the processing gain and the reduction of this gain ascribable to the window for tones matched to the basis vectors. The basis vectors are tones with frequencies equal to multiples of  $f_s/N$  (with  $f_s$  being the sample frequency). These frequencies are sample points from the spectrum, and are normally referred to as DFT output points or as DFT bins. We now address the question, what is the additional loss in processing gain for a tone of frequency midway between two bin frequencies (that is, at frequencies  $(k + 1/2)f_s/N$ )?

Returning to (13), with  $\omega_k$  replaced by  $\omega_{(k+1/2)}$ , we determine the processing gain for this half-bin frequency shift as defined in

$$F(\omega_{(1/2)})|_{\text{signal}} = A \sum_n w(nT) \exp(-j\omega_{(1/2)}nT),$$

$$\text{where } \omega_{(1/2)} = \frac{1}{2} \frac{\omega_s}{N} = \frac{\pi}{NT}. \quad (20a)$$

We also define the scalping loss as the ratio of coherent gain for a tone located half a bin from a DFT sample point to the coherent gain for a tone located at a DFT sample point, as indicated in

$$\text{Scalping Loss} = \frac{\left| \sum_n w(nT) \exp\left(-j\frac{\pi}{N}n\right) \right|}{\sum_n w(nT)} = \frac{\left| W\left(\frac{1}{2} \frac{\omega_s}{N}\right) \right|}{W(0)}.$$

(20b)

Scalping loss represents the maximum reduction in PG due to signal frequency. This loss has been computed for the windows of this report and has been included in Table I.

#### E. Worst Case Processing Loss

We now make an interesting observation. We define worst case PL as the sum of maximum scalping loss of a window and of PL due to that window (both in decibel). This number is the reduction of output signal-to-noise ratio as a result of windowing and of worst case frequency location. This of course is related to the minimum detectable tone in broadband noise. It is interesting to note that the worst case loss is always between 3.0 and 4.3 dB. Windows with worst case PL exceeding 3.8 dB are very poor windows and should not

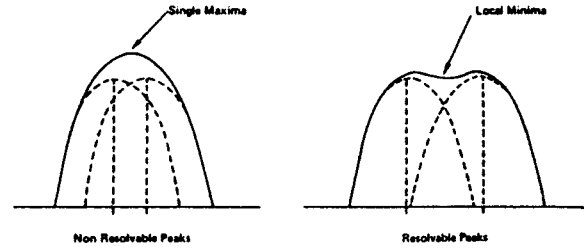


Fig. 11. Spectral resolution of nearby kernels.

be used. Additional comments on poor windows will be found in Section IV-G. We can conclude from the combined loss figures of Table I and from Fig. 12 that for the detection of single tones in broad-band noise, nearly any window (other than the rectangle) is as good as any other. The difference between the various windows is less than 1.0 dB and for good windows is less than 0.7 dB. The detection of tones in the presence of other tones is, however, quite another problem. Here the window does have a marked affect, as will be demonstrated shortly.

#### F. Spectral Leakage Revisited

Returning to (6) and to Fig. 6, we observe the spectral measurement is affected not only by the broadband noise spectrum, but also by the narrow-band spectrum which falls within the bandwidth of the window. In fact, a given spectral component say at  $\omega = \omega_0$  will contribute output (or will be observed) at another frequency, say at  $\omega = \omega_a$  according to the gain of the window centered at  $\omega_0$  and measured at  $\omega_a$ . This is the effect normally referred to as spectral leakage and is demonstrated in Fig. 10 with the transform of a finite duration tone of frequency  $\omega_0$ .

This leakage causes a bias in the amplitude and the position of a harmonic estimate. Even for the case of a single real harmonic line (not at a DFT sample point), the leakage from the kernel on the negative-frequency axis biases the kernel on the positive-frequency line. This bias is most severe and most bothersome for the detection of small signals in the presence of nearby large signals. To reduce the effects of this bias, the window should exhibit low-amplitude sidelobes far from the central main lobe, and the transition to the low sidelobes should be very rapid. One indicator of how well a window suppresses leakage is the peak sidelobe level (relative to the main lobe): another is the asymptotic rate of falloff of these sidelobes. These indicators are listed in Table I.

#### G. Minimum Resolution Bandwidth

Fig. 11 suggests another criterion with which we should be concerned in the window selection process. Since the window imposes an effective bandwidth on the spectral line, we would be interested in the minimum separation between two equal-strength lines such that for arbitrary spectral locations their respective main lobes can be resolved. The classic criterion for this resolution is the width of the window at the half-power points (the 3.0-dB bandwidth). This criterion reflects the fact that two equal-strength main lobes separated in frequency by less than their 3.0-dB bandwidths will exhibit a single spectral peak and will not be resolved as two distinct lines. The problem with this criterion is that it does not work for the coherent addition we find in the DFT. The DFT output points are the coherent addition of the spectral components weighted through the window at a given frequency.



If two kernels are contributing to the coherent summation, the sum at the crossover point (nominally half-way between them) must be smaller than the individual peaks if the two peaks are to be resolved. Thus at the crossover points of the kernels, the gain from each kernel must be less than 0.5, or the crossover points must occur beyond the 6.0-dB points of the windows. Table I lists the 6.0-dB bandwidths of the various windows examined in this report. From the table, we see that the 6.0-dB bandwidth varies from 1.2 bins to 2.6 bins, where a bin is the fundamental frequency resolution  $\omega_s/N$ . The 3.0-dB bandwidth does have utility as a performance indicator as shown in the next paragraph. Remember however, it is the 6.0-dB bandwidth which defines the resolution of the windowed DFT.

From Table I, we see that the noise bandwidth always exceeds the 3.0-dB bandwidth. The difference between the two, referenced to the 3.0-dB bandwidth, appears to be a sensitive indicator of overall window performance. We have observed that for all the good windows on the table, this indicator was found to be in the range of 4.0 to 5.5 percent. Those windows for which this ratio is outside that range either have a wide main lobe or a high sidelobe structure and, hence, are characterized by high processing loss or by poor two-tone detection capabilities. Those windows for which this ratio is inside the 4.0 to 5.5-percent range are found in the lower left corner of the performance comparison chart (Fig. 12), which is described next.

While Table I does list the common performance parameters of the windows examined in this report, the mass of numbers is not enlightening. We do realize that the sidelobe level (to reduce bias) and the worst case processing loss (to maximize detectability) are probably the most important parameters on the table. Fig. 12 shows the relative position of the windows as a function of these parameters. Windows residing in the lower left corner of the figure are the good-performing windows. They exhibit low-sidelobe levels and low worst case processing loss. We urge the reader to read Sections VI and VII; Fig. 12 presents a lot of information, but not the full story.

## V. CLASSIC WINDOWS

We will now catalog some well-known (and some not well-known) windows. For each window we will comment on the justification for its use and identify its significant parameters. All the windows will be presented as even (about the origin) sequences with an odd number of points. To convert the window to DFT-even, the right end point will be discarded and the sequence will be shifted so that the left end point coincides with the origin. We will use normalized coordinates with sample period  $T = 1.0$ , so that  $\omega$  is periodic in  $2\pi$  and, hence, will be identified as  $\theta$ . A DFT bin will be considered to extend between DFT sample points (multiples of  $2\pi/N$ ) and have a width of  $2\pi/N$ .

### A. Rectangle (Dirichlet) Window [6]

The rectangle window is unity over the observation interval, and can be thought of as a gating sequence applied to the data so that they are of finite extent. The window for a finite Fourier transform is defined as

$$w(n) = 1.0, \quad n = -\frac{N}{2}, \dots, -1, 0, 1, \dots, \frac{N}{2} \quad (21a)$$

and is shown in Fig. 13. The same window for a DFT is

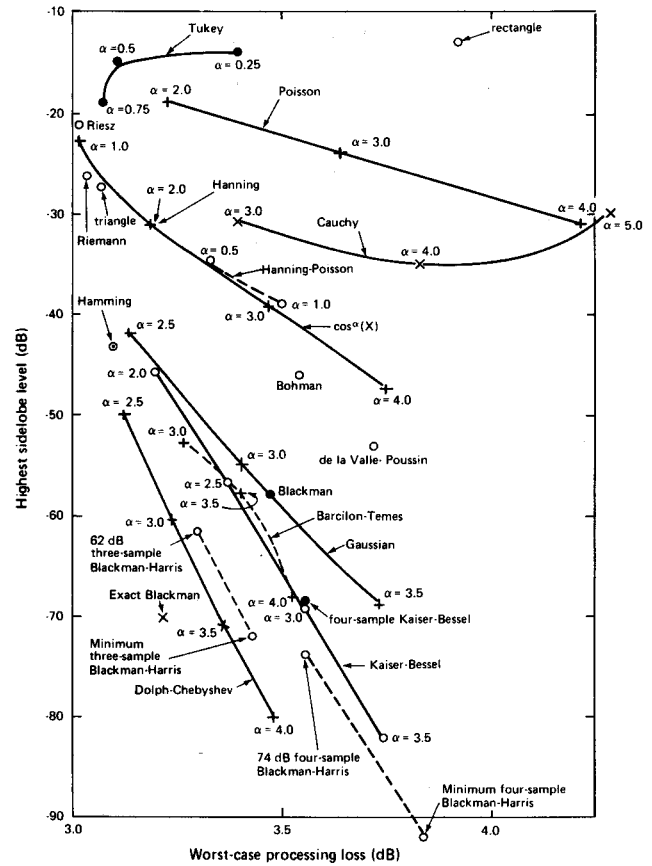


Fig. 12. Comparison of windows: sidelobe levels and worst case processing loss.

defined as

$$w(n) = 1.0, \quad n = 0, 1, \dots, N-1. \quad (21b)$$

The spectral window for the DFT window sequence is given in

$$W(\theta) = \exp \left( -j \frac{N-1}{2} \theta \right) \frac{\sin \left[ \frac{N}{2} \theta \right]}{\sin \left[ \frac{1}{2} \theta \right]}. \quad (21c)$$

The transform of this window is seen to be the Dirichlet kernel, which exhibits a DFT main-lobe width (between zero crossings) of 2 bins and a first sidelobe level approximately 13 dB down from the main-lobe peak. The sidelobes fall off at 6.0 dB per octave, which is of course the expected rate for a function with a discontinuity. The parameters of the DFT window are listed in Table I.

With the rectangle window now defined, we can answer the question posed earlier: in what sense does the finite sum of (22a) approximate the infinite sum of (22b)?

$$F(\theta) = \sum_{n=-N/2}^{+N/2} f(n) \exp(-jn\theta) \quad (22a)$$

$$F(\theta) = \sum_{n=-\infty}^{+\infty} f(n) \exp(-jn\theta). \quad (22b)$$

We observe the finite sum is the rectangle-windowed version of the infinite sum. We recognize that the infinite sum is the Fourier series expansion of some periodic function for which the  $f(n)$ 's are the Fourier series coefficients. We also recognize

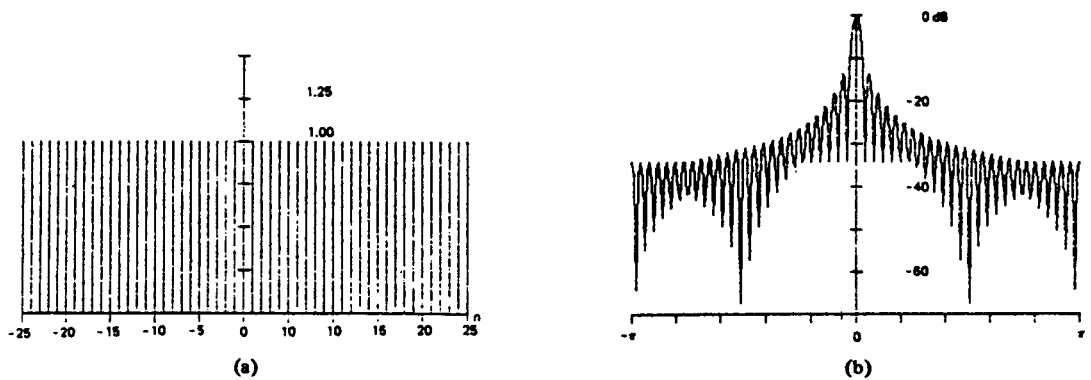


Fig. 13. (a) Rectangle window. (b) Log-magnitude of transform.

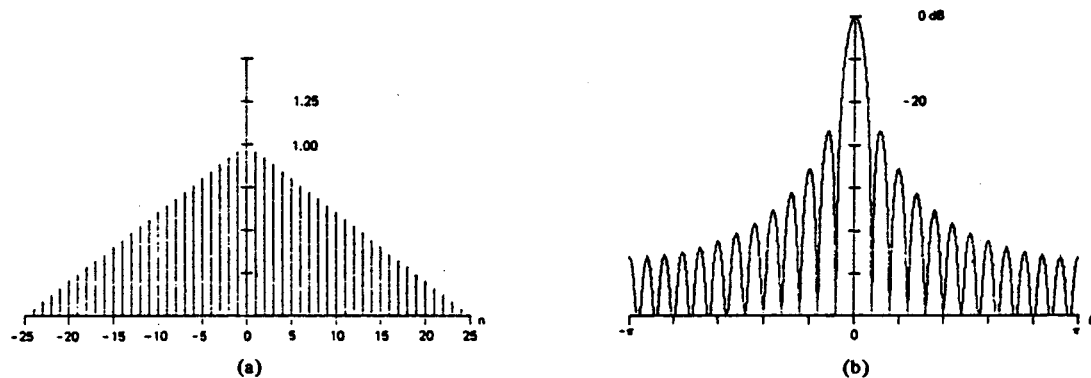


Fig. 14. (a) Triangle window. (b) Log-magnitude of transform.

that the finite sum is simply the partial sum of the series. From this viewpoint we can cast the question in terms of the convergence properties of the partial sums of Fourier series. From this work we know the partial sum is the least mean-square error approximation to the infinite sum.

We observe that mean square convergence is a convenient analytic concept, but it is not attractive for finite estimates or for numerical approximations. Mean-square estimates tend to oscillate about their means, and do not exhibit uniform convergence. (The approximation in a neighborhood of a point of continuity may get worse if more terms are added to the partial sum.) We normally observe this behavior near points of discontinuity as the ringing we call Gibbs phenomenon. It is this oscillatory behavior we are trying to control by the use of other windows.

#### B. Triangle (Fejer, Bartlett) Window [7]

The triangle window for a finite Fourier transform is defined as

$$W(n) = 1.0 - \frac{|n|}{N/2}, \quad n = -\frac{N}{2}, \dots, -1, 0, 1, \dots, \frac{N}{2} \quad (23a)$$

and is shown in Fig. 14. The same window for a DFT is defined as

$$W(n) = \begin{cases} \frac{n}{N/2}, & n = 0, 1, \dots, \frac{N}{2} \\ W(N-n), & n = \frac{N}{2}, \dots, N-1 \end{cases} \quad (23b)$$

and the spectral window corresponding to the DFT sequence is given in

$$W(\theta) = \frac{2}{N} \exp \left[ -j \left( \frac{N}{2} - 1 \right) \theta \right] \left[ \frac{\sin \left( \frac{N}{4} \theta \right)}{\sin \left( \frac{1}{2} \theta \right)} \right]^2 \quad (23c)$$

The transform of this window is seen to be the squared Dirichlet kernel. Its main-lobe width (between zero crossings) is twice that of the rectangle's and the first sidelobe level is approximately 26 dB down from the main-lobe peak, again, twice that of the rectangle's. The sidelobes fall off at -12 dB per octave, reflecting the discontinuity of the window residing in the first derivative (rather than in the function itself). The triangle is the simplest window which exhibits a nonnegative transform. This property can be realized by convolving any window (of half-extent) with itself. The resultant window's transform is the square of the original window's transform.

A window sequence derived by self-convolving a parent window contains approximately twice the number of samples as the parent window, hence corresponds to a trigonometric polynomial (its Z-transform) of approximately twice the order. (Convoluting two rectangles each of  $N/2$  points will result in a triangle of  $N+1$  points when the zero end points are counted.) The transform of the window will now exhibit twice as many zeros as the parent transform (to account for the increased order of the associated trigonometric polynomial). But how has the transform applied these extra zeros available from the increased order polynomial? The self-

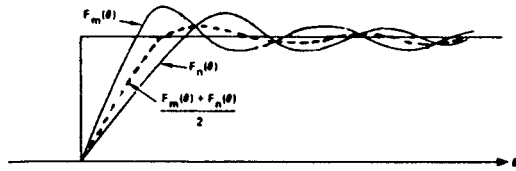


Fig. 15. Two partial sums and their average.

 TABLE II  
FEJER CONVERGENCE FACTORS AS AN AVERAGE TRANSFORM

$F_0(\theta)$	$f_0$								
$F_1(\theta)$			$f_{-1}$	$f_0$	$f_{+1}$				
$F_2(\theta)$			$f_{-2}$	$f_{-1}$	$f_0$	$f_{+1}$	$f_{+2}$		
$F_3(\theta)$			$f_{-3}$	$f_{-2}$	$f_{-1}$	$f_0$	$f_{+1}$	$f_{+2}$	$f_{+3}$
$F^4(\theta)$	$\frac{0}{4}f_{-4}$	$\frac{1}{4}f_{-3}$	$\frac{2}{4}f_{-2}$	$\frac{3}{4}f_{-1}$	$\frac{4}{4}f_0$	$\frac{3}{4}f_{+1}$	$\frac{2}{4}f_{+2}$	$\frac{1}{4}f_{+3}$	$\frac{0}{4}f_{+4}$

convolved window simply places repeated zeros at each location for which the parent transform had a zero. This, of course, not only sets the transform to zero at those points, but also sets the first derivative to zero at those points. If the intent of the increased order of polynomial is to hold down the sidelobe levels, then doubling up on the zeros is a wasteful tactic. The additional zeros might better be placed between the existing zeros (near the local peaks of the sidelobes) to hold down the sidelobes rather than at locations for which the transform is already equal to zero. In fact we will observe in subsequent windows that very few good windows exhibit repeated roots.

Backing up for a moment, it is interesting to examine the triangle window in terms of partial-sum convergence of Fourier series. Fejer observed that the partial sums of Fourier series were poor numerical approximations [8]. Fourier coefficients were easy to generate however, and he questioned if some simple modification of coefficients might lead to a new set with more desirable convergence properties. The oscillation of the partial sum, and the contraction of those oscillations as the order of the partial sum increased, suggested that an average of the partial sums would be a smoother function. Fig. 15 presents an expansion of two partial sums near a discontinuity. Notice the average of the two expansions is smoother than either. Continuing in this line of reasoning, an average expansion  $F^N(\theta)$  might be defined by

$$F^N(\theta) = \frac{1}{N} [F_{N-1}(\theta) + F_{N-2}(\theta) + \cdots + F_0(\theta)] \quad (24)$$

where  $F_M(\theta)$  is the  $M$ -term partial sum of the series. This is easily visualized in Table II, which lists the nonzero coefficients of the first four partial sums and their average summation. We see that the Fejer convergence factors applied to the Fourier series coefficients is, in fact, a triangle window. The averaging of partial sums is known as the method of Cesàro summability.

### C. $\cos^\alpha(X)$ Windows

This is actually a family of windows dependent upon the parameter  $\alpha$ , with  $\alpha$  normally being an integer. Attractions of this family include the ease with which the terms can be generated, and the easily identified properties of the transform

of the cosine function. These properties are particularly attractive under the DFT. The window for a finite Fourier transform is defined as

$$w(n) = \cos^\alpha \left[ \frac{n}{N} \pi \right], \quad n = -\frac{N}{2}, \cdots, -1, 0, 1, \cdots, \frac{N}{2} \quad (25a)$$

and for a DFT as

$$w(n) = \sin^\alpha \left[ \frac{n}{N} \pi \right], \quad n = 0, 1, 2, \cdots, N-1. \quad (25b)$$

Notice the effect due to the change of the origin. The most common values of  $\alpha$  are the integers 1 through 4, with 2 being the most well known (as the Hanning window). This window is identified for values of  $\alpha$  equal to 1 and 2 in (26a), (26b), (27a), and (27b), (the "a" for the finite transforms, the "b" for the DFT):

$\alpha = 1.0$  (cosine lobe)

$$w(n) = \cos \left[ \frac{n}{N} \pi \right], \quad n = -\frac{N}{2}, \cdots, -1, 0, 1, \cdots, \frac{N}{2} \quad (26a)$$

$\alpha = 1.0$  (sine lobe)

$$w(n) = \sin \left[ \frac{n}{N} \pi \right], \quad n = 0, 1, 2, \cdots, N-1 \quad (26b)$$

$\alpha = 2.0$  (cosine squared, raised cosine, Hanning)

$$w(n) = \cos^2 \left[ \frac{n}{N} \pi \right] = 0.5 \left[ 1.0 + \cos \left[ \frac{2n}{N} \pi \right] \right], \quad n = -\frac{N}{2}, \cdots, -1, 0, 1, \cdots, \frac{N}{2} \quad (27a)$$

$\alpha = 2.0$  (sine squared, raised cosine, Hanning)

$$w(n) = \sin^2 \left[ \frac{n}{N} \pi \right] = 0.5 \left[ 1.0 - \cos \left[ \frac{2n}{N} \pi \right] \right], \quad n = 0, 1, 2, \cdots, N-1. \quad (27b)$$

The windows are shown for  $\alpha$  integer values of 1 through 4 in Figs. 16 through 19. Notice as  $\alpha$  becomes larger, the windows become smoother and the transform reflects this increased smoothness in decreased sidelobe level and faster falloff of the sidelobes, but with an increased width of the main lobe.

Of particular interest in this family, is the Hann window (after the Austrian meteorologist, Julius Von Hann)<sup>1</sup> [7]. Not only is this window continuous, but so is its first derivative. Since the discontinuity of this window resides in the second derivative, the transform falls off at  $1/\omega^3$  or at -18 dB per octave. Let us closely examine the transform of this window. We will gain some interesting insight and learn of a clever application of the window under the DFT.

<sup>1</sup>The correct name of this window is "Hann." The term "Hanning" is used in this report to reflect conventional usage. The derived term "Hann'd" is also widely used.

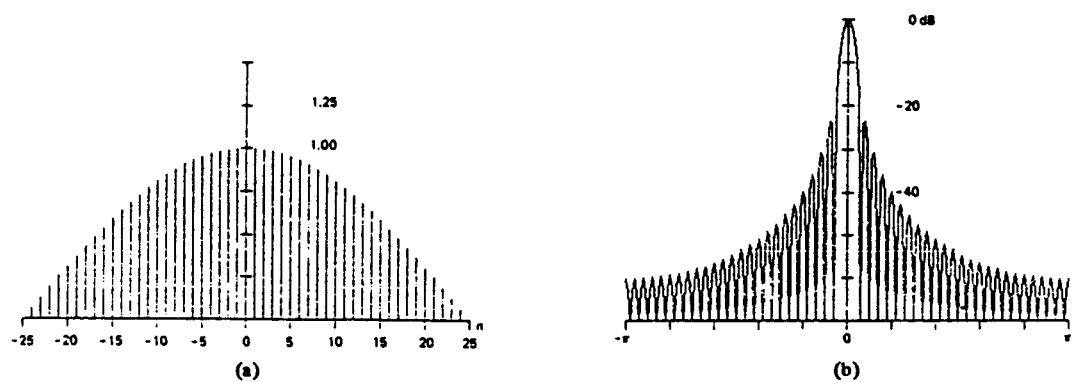


Fig. 16. (a)  $\cos(n\pi/N)$  window. (b) Log-magnitude of transform.

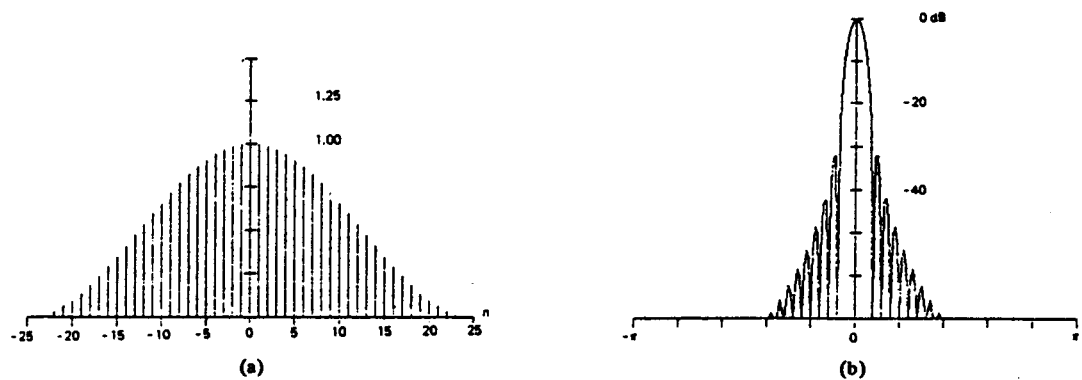


Fig. 17. (a)  $\cos^2(n\pi/N)$  window. (b) Log-magnitude of transform.

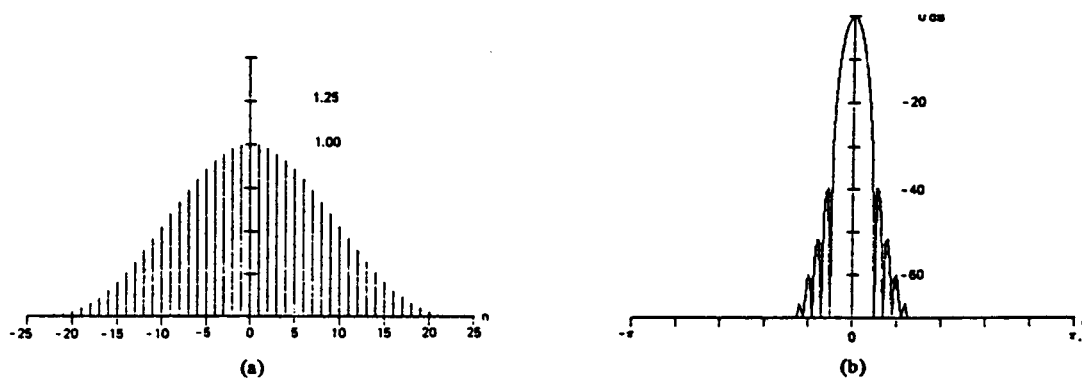


Fig. 18. (a)  $\cos^3(n\pi/N)$  window. (b) Log-magnitude of transform.

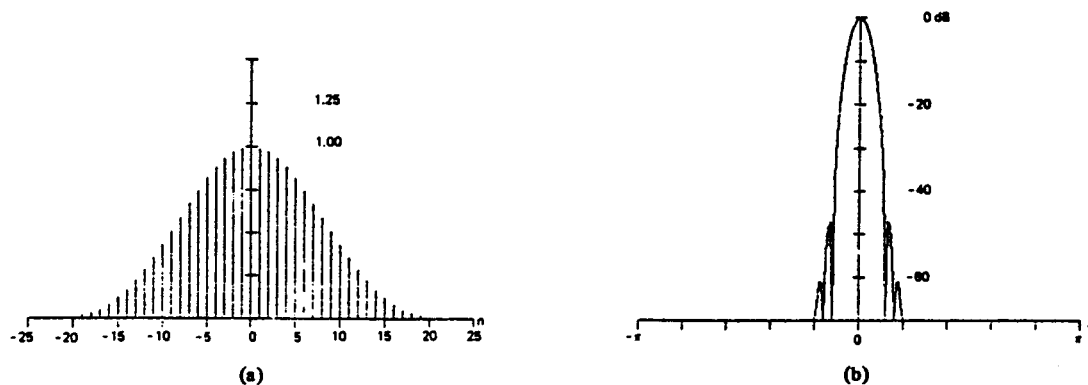


Fig. 19. (a)  $\cos^4(n\pi/N)$  window. (b) Log-magnitude of transform.

The sampled Hanning window can be written as the sum of the sequences indicated in

$$w(n) = 0.5 + 0.5 \cos \left[ \frac{2n}{N} \pi \right], \quad n = -\frac{N}{2}, \dots, -1, 0, 1, \dots, \frac{N}{2} - 1. \quad (28a)$$

Each sequence has the easily recognized DFT indicated in

$$W(\theta) = 0.5 D(\theta) + 0.25 \left[ D\left(\theta - \frac{2\pi}{N}\right) + D\left(\theta + \frac{2\pi}{N}\right) \right] \quad (28b)$$

where

$$D(\theta) = \exp \left( +j \frac{\theta}{2} \right) \frac{\sin \left[ \frac{N}{2} \theta \right]}{\sin \left[ \frac{1}{2} \theta \right]}.$$

We recognize the Dirichlet kernel at the origin as the transform of the constant 0.5 samples and the pair of translated kernels as the transform of the single cycle of cosine samples. Note that the translated kernels are located on the first zeros of the center kernel, and are half the size of the center kernel. Also the sidelobes of the translated kernel are about half the size and are of opposite phase of the sidelobes of the central kernel. The summation of the three kernels' sidelobes being in phase opposition, tends to cancel the sidelobe structure. This cancelling summation is demonstrated in Fig. 20 which depicts the summation of the Dirichlet kernels (without the phase-shift terms).

The partial cancelling of the sidelobe structure suggests a constructive technique to define new windows. The most well-known of these are the Hamming and the Blackman windows which are presented in the next two sections.

For the special case of the DFT, the Hanning window is sampled at multiples of  $2\pi/N$ , which of course are the locations of the zeros of the central Dirichlet kernel. Thus only three nonzero samples are taken in the sampling process. The positions of these samples are at  $-2\pi/N$ , 0, and  $+2\pi/N$ . The value of the samples obtained from (28b) (including the phase factor  $\exp(-j(N/2)\theta)$  to account for the  $N/2$  shift) are  $-\frac{1}{4}$ ,  $+\frac{1}{2}$ ,  $-\frac{1}{4}$ , respectively. Note the minus signs. These results from the shift in the origin for the window. Without the shift, the phase term is missing and the coefficients are all positive  $\frac{1}{4}$ ,  $\frac{1}{2}$ ,  $\frac{1}{4}$ . These are incorrect for DFT processing, but they find their way into much of the literature and practice.

Rather than apply the window as a product in the time domain, we always have the option to apply it as a convolution in the frequency domain. The attraction of the Hanning window for this application is twofold; first, the window spectra is nonzero at only three data points, and second, the sample values are binary fractions, which can be implemented as right shifts. Thus the Hanning-windowed spectral points obtained from the rectangle-windowed spectral points are obtained as indicated in the following equation as two real adds and two binary shifts (to multiply by  $\frac{1}{2}$ ):

$$F(k) \Big|_{\text{Hanning}} = \frac{1}{2} [F(k) - \frac{1}{2} [F(k-1) + F(k+1)]] \Big|_{\text{Rectangle}}. \quad (29)$$

Thus a Hanning window applied to a real transform of length  $N$  can be performed as  $N$  real multiplies on the time sequence

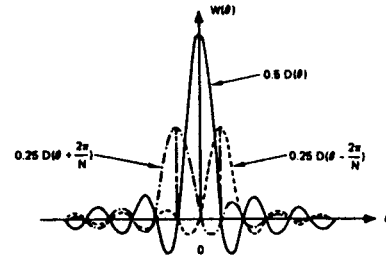


Fig. 20. Transform of Hanning window as a sum of three Dirichlet kernels.

or as  $2N$  real adds and  $2N$  binary shifts on the spectral data. One other mildly important consideration, if the window is to be applied to the time data, is that the samples of the window must be stored somewhere, which normally means additional memory or hardware. It so happens that the samples of the cosine for the Hanning window are already stored in the machine as the trig-table for the FFT; thus the Hanning window requires no additional storage.

#### D. Hamming Window [7]

The Hamming window can be thought of as a modified Hanning window. (Note the potential source of confusion in the similarities of the two names.) Referring back to Figs. 17 and 20, we note the inexact cancellation of the sidelobes from the summation of the three kernels. We can construct a window by adjusting the relative size of the kernels as indicated in the following to achieve a more desirable form of cancellation:

$$w(n) = \alpha + (1 - \alpha) \cos \left[ \frac{2\pi}{N} n \right] \quad (30a)$$

$$W(\theta) = \alpha D(\theta) + 0.5 (1 - \alpha) \left[ D\left(\theta - \frac{2\pi}{N}\right) + D\left(\theta + \frac{2\pi}{N}\right) \right].$$

Perfect cancellation of the first sidelobe (at  $\theta = 2.5 [2\pi/N]$ ) occurs when  $\alpha = 25/46$  ( $\alpha \approx 0.543 478 261$ ). If  $\alpha$  is selected as 0.54 (an approximation to  $25/46$ ), the new zero occurs at  $\theta \approx 2.6 [2\pi/N]$  and a marked improvement in sidelobe level is realized. For this value of  $\alpha$ , the window is called the Hamming window and is identified by

$$w(n) = \begin{cases} 0.54 + 0.46 \cos \left[ \frac{2\pi}{N} n \right], & n = -\frac{N}{2}, \dots, -1, 0, 1, \dots, \frac{N}{2} \\ 0.54 - 0.46 \cos \left[ \frac{2\pi}{N} n \right], & n = 0, 1, 2, \dots, N-1. \end{cases} \quad (30b)$$

The coefficients of the Hamming window are nearly the set which achieve minimum sidelobe levels. If  $\alpha$  is selected to be 0.53856 the sidelobe level is  $-43$  dB and the resultant window is a special case of the Blackman-Harris windows presented in Section V-E. The Hamming window is shown in Fig. 21. Notice the deep attenuation at the missing sidelobe position. Note also that the small discontinuity at the boundary of the window has resulted in a  $1/\omega$  (6.0 dB per octave) rate of falloff. The better sidelobe cancellation does result in a much lower initial sidelobe level of  $-42$  dB. Table I lists the param-

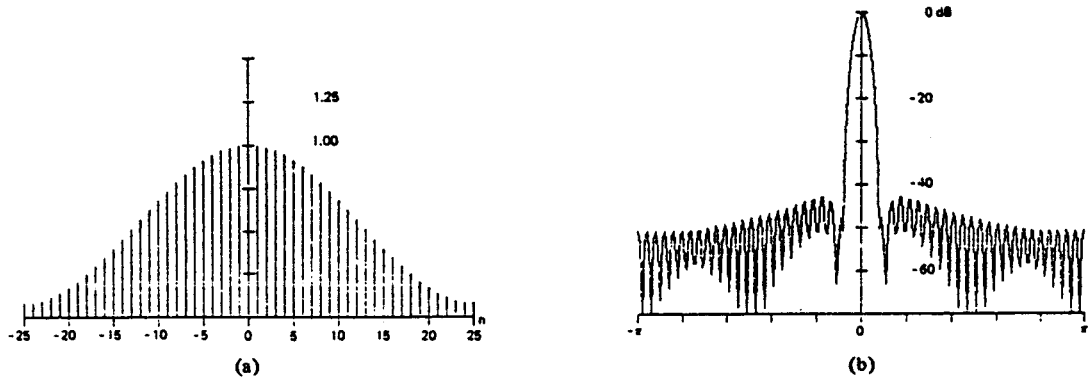


Fig. 21. (a) Hamming window. (b) Log-magnitude of Fourier transform.

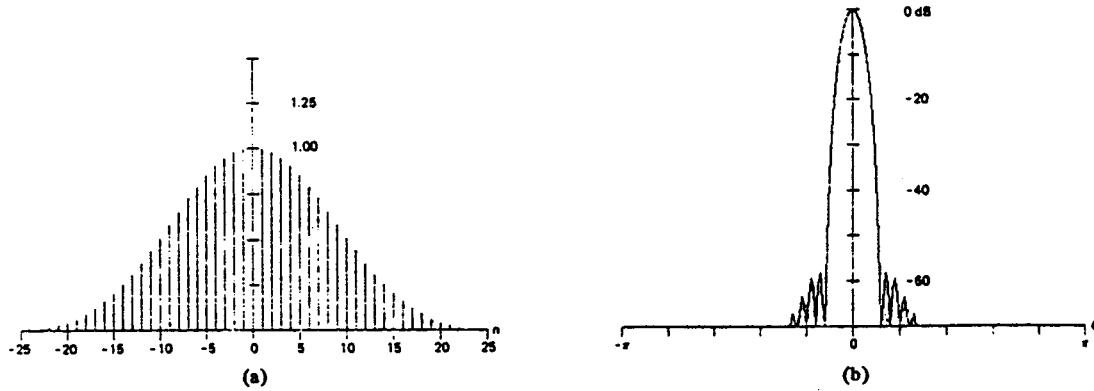


Fig. 22. (a) Blackman window. (b) Log-magnitude of transform.

eters of this window. Also note the loss of binary weighting; hence the need to perform multiplication to apply the weighting factors of the spectral convolution.

#### E. Blackman Window [7]

The Hamming and Hanning windows are examples of windows constructed as the summation of shifted Dirichlet kernels. This data window is defined for the finite Fourier transform in (31a) and for the DFT in (31b); equation (31c) is the resultant spectral window for the DFT given as a summation of the Dirichlet kernels  $D(\theta)$  defined by  $W(\theta)$  in (21c);

$$W(n) = \sum_{m=0}^{N/2} a_m \cos \left[ \frac{2\pi}{N} mn \right], \quad n = -\frac{N}{2}, \dots, -1, 0, 1, \dots, \frac{N}{2} \quad (31a)$$

$$W(n) = \sum_{m=0}^{N/2} (-1)^m a_m \cos \left[ \frac{2\pi}{N} mn \right], \quad n = 0, 1, \dots, N-1 \quad (31b)$$

$$W(\theta) = \sum_{m=0}^{N/2} (-1)^m \frac{a_m}{2} \left[ D \left( \theta - \frac{2\pi}{N} m \right) + D \left( \theta + \frac{2\pi}{N} m \right) \right]. \quad (31c)$$

Subject to constraint

$$\sum_{m=0}^{N/2} a_m = 1.0.$$

We can see that the Hanning and the Hamming windows are

of this form with  $a_0$  and  $a_1$  being nonzero. We see that their spectral windows are summations of three-shifted kernels.

We can construct windows with any  $K$  nonzero coefficients and achieve a  $(2K-1)$  summation of kernels. We recognize, however, that one way to achieve windows with a narrow main lobe is to restrict  $K$  to a small integer. Blackman examined this window for  $K=3$  and found the values of the nonzero coefficients which place zeros at  $\theta = 3.5 (2\pi/N)$  and at  $\theta = 4.5 (2\pi/N)$ , the position of the third and the fourth sidelobes, respectively, of the central Dirichlet kernel. These exact values and their two place approximations are

$$a_0 = \frac{7938}{18608} \doteq 0.426 \, 590 \, 71 \approx 0.42$$

$$a_1 = \frac{9240}{18608} \doteq 0.496 \, 560 \, 62 \approx 0.50$$

$$a_2 = \frac{1430}{18608} \doteq 0.076 \, 848 \, 67 \approx 0.08.$$

The window which uses these two place approximations is known as the Blackman window. When we describe this window with the "exact" coefficients we will refer to it as the exact Blackman window. The Blackman window is defined for the finite transform in the following equation and the window is shown in Fig. 22:

$$W(n) = 0.42 + 0.50 \cos \left[ \frac{2\pi}{N} n \right] + 0.08 \cos \left[ \frac{2\pi}{N} 2n \right], \quad n = -\frac{N}{2}, \dots, -1, 0, 1, \dots, \frac{N}{2}. \quad (32)$$

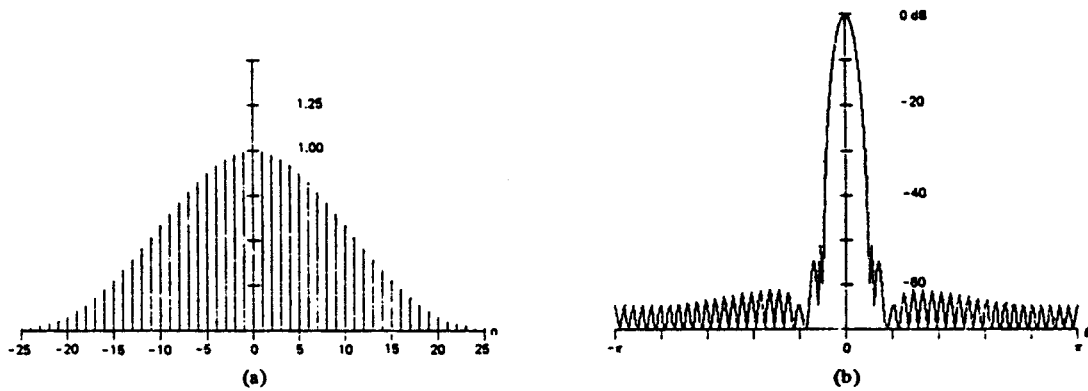


Fig. 23. (a) Exact Blackman window. (b) Log-magnitude of transform.

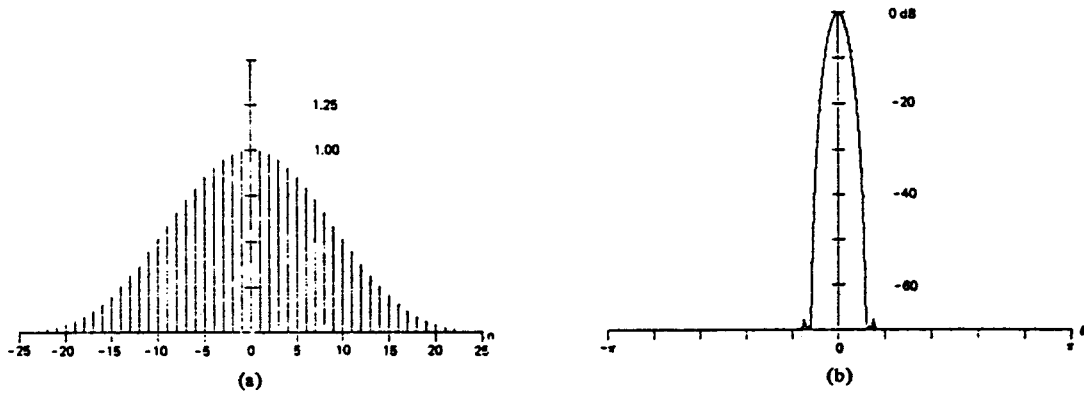


Fig. 24. (a) Minimum 3-term Blackman-Harris window. (b) Log-magnitude of transform.

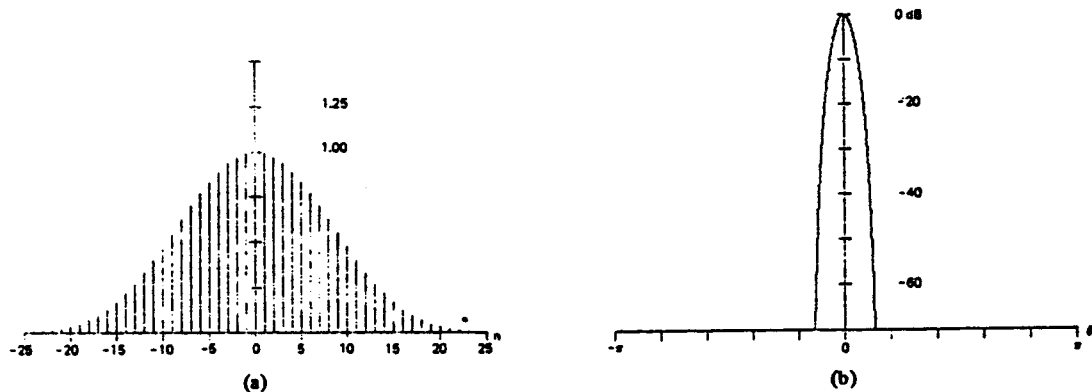


Fig. 25. (a) 4-term Blackman-Harris window. (b) Log-magnitude of transform.

The exact Blackman window is shown in Fig. 23. The sidelobe level is 51 dB down for the exact Blackman window and is 58 dB down for the Blackman window. As an observation, note that the coefficients of the Blackman window sum to zero ( $0.42 - 0.50 + 0.08$ ) at the boundaries while the exact coefficients do not. Thus the Blackman window is continuous with a continuous first derivative at the boundary and falls off like  $1/\omega^3$  or 18 dB per octave. The exact terms (like the Hamming window) have a discontinuity at the boundary and falls off like  $1/\omega$  or 6 dB per octave. Table I lists the parameters of these two windows. Note that for this class of windows, the  $a_0$  coefficient is the coherent gain of the window.

Using a gradient search technique [9], we have found the windows which for 3- and 4-nonzero terms achieve a minimum

sidelobe level. We have also constructed families of 3- and 4-term windows in which we trade main-lobe width for sidelobe level. We call this family the Blackman-Harris window. We have found that the minimum 3-term window can achieve a sidelobe level of -67 dB and that the minimum 4-term window can achieve a sidelobe level of -92 dB. These windows are defined for the DFT by

$$w(n) = a_0 - a_1 \cos\left(\frac{2\pi}{N}n\right) + a_2 \cos\left(\frac{2\pi}{N}2n\right) - a_3 \cos\left(\frac{2\pi}{N}3n\right),$$

$$n = 0, 1, 2, \dots, N-1. \quad (33)$$

The listed coefficients correspond to the minimum 3-term window which is presented in Fig. 24, another 3-term window

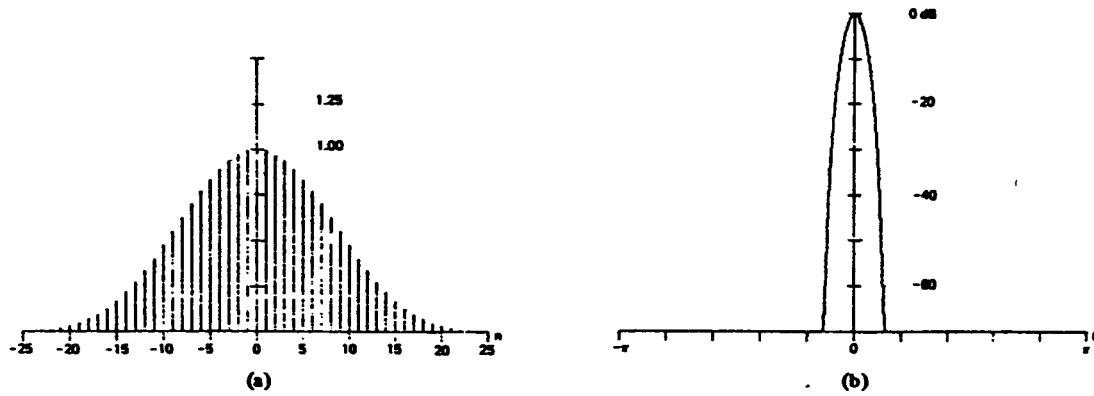


Fig. 26. (a) 4-sample Kaiser-Bessel window. (b) Log-magnitude of transform.

	3-Term (-67 dB)	3-Term (-61 dB)	4-Term (-92 dB)	4-Term (-74 dB)
$a_0$	0.42323	0.44959	0.35875	0.40217
$a_1$	0.49755	0.49364	0.48829	0.49703
$a_2$	0.07922	0.05677	0.14128	0.09392
$a_3$	---	---	0.01168	0.00183

(to establish another data point in Fig. 12), the minimum 4-term window (to also establish a data point in Fig. 12), and another 4-term window which is presented in Fig. 25. The particular 4-term window shown is one which performs well in a detection example described in Section VI (see Fig. 69). The parameters of these windows are listed in Table I. Note in particular where the Blackman and the Blackman-Harris windows reside in Fig. 12. They are surprisingly good windows for the small number of terms in their trigonometric series. Note, if we were to extend the line connecting the Blackman-Harris family it would intersect the Hamming window which, in Section V-D, we noted is nearly the minimum sidelobe level 2-term Blackman-Harris window.

We also mention that a good approximation to the Blackman-Harris 3- and 4-term windows can be obtained as scaled samples of the Kaiser-Bessel window's transform (see Section V-H). We have used this approximation to construct 4-term windows for adjustable bandwidth convolutional filters as reported in [10]. This approximation is defined as

$$b_m = \frac{\sinh[\pi\sqrt{\alpha^2 - m^2}]}{\pi\sqrt{\alpha^2 - m^2}}, \quad m \leq \alpha, \quad 2 \leq \alpha < 4$$

$$c = b_0 + 2b_1 + 2b_2 + (2b_3)$$

$$a_0 = \frac{b_0}{c}, \quad a_m = 2\frac{b_m}{c}, \quad m = 1, 2, (3). \quad (34)$$

The 4 coefficients for this approximation when  $\alpha = 3.0$  are  $a_0 = 0.40243$ ,  $a_1 = 0.49804$ ,  $a_2 = 0.09831$ , and  $a_3 = 0.00122$ . Notice how close these terms are to the selected 4-term Blackman-Harris (-74 dB) window. The window defined by these coefficients is shown in Fig. 26. Like the prototype from which it came (the Kaiser-Bessel with  $\alpha = 3.0$ ), this window exhibits sidelobes just shy of -70 dB from the main lobe. On the scale shown, the two are indistinguishable. The parameters of this window are also listed in Table I and the window is entered in Fig. 12 as the "4-sample Kaiser-Bessel." It was these 3- and 4-sample Kaiser-Bessel prototype

windows (parameterized on  $\alpha$ ) which were the starting conditions for the gradient minimization which leads to the Blackman-Harris windows. The optimization starting with these coefficients has virtually no effect on the main-lobe characteristics but does drive down the sidelobes approximately 5 dB.

#### F. Constructed Windows

Numerous investigators have constructed windows as products, as sums, as sections, or as convolutions of simple functions and of other simple windows. These windows have been constructed for certain desirable features, not the least of which is the attraction of simple functions for generating the window terms. In general, the constructed windows tend not to be good windows, and occasionally are very bad windows. We have already examined some simple window constructions. The Fejer (Bartlett) window, for instance, is the convolution of two rectangle windows; the Hamming window is the sum of a rectangle and a Hanning window; and the  $\cos^4(X)$  window is the product of two Hanning windows. We will now examine other constructed windows that have appeared in the literature. We will present them so they are available for comparison. Later we will examine windows constructed in accord with some criteria of optimality (see Sections V-G, H, I, and J). Each window is identified only for the finite Fourier transform. A simple shift of  $N/2$  points and right end-point deletion will supply the DFT version. The significant figures of performance for these windows are also found in Table I.

1) *Riesz (Bochner, Parzen) Window* [11]: The Riesz window, identified as

$$w(n) = 1.0 - \left| \frac{n}{N/2} \right|^2, \quad 0 \leq |n| \leq \frac{N}{2} \quad (35)$$

is the simplest continuous polynomial window. It exhibits a discontinuous first derivative at the boundaries; hence its transform falls off like  $1/\omega^2$ . The window is shown in Fig. 27. The first sidelobe is -22 dB from the main lobe. This window is similar to the cosine lobe (26) as can be demonstrated by examining its Taylor series expansion.

2) *Riemann Window* [12]: The Riemann window, defined by

$$w(n) = \frac{\sin\left[\frac{n}{N}2\pi\right]}{\left[\frac{n}{N}2\pi\right]}, \quad 0 \leq |n| \leq \frac{N}{2} \quad (36)$$

is the central lobe of the SINC kernel. This window is con-



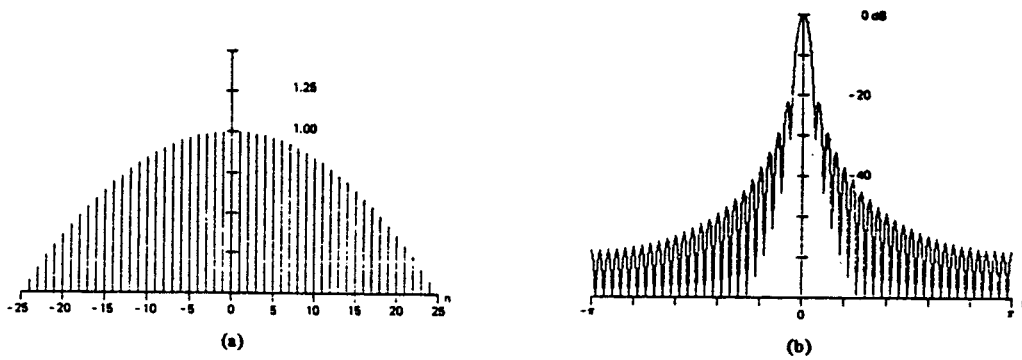


Fig. 27. (a) Riesz window. (b) Log-magnitude of transform.

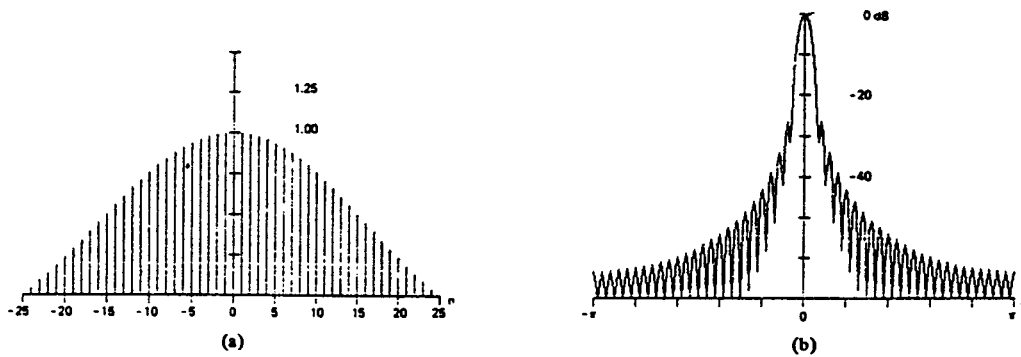


Fig. 28. (a) Riemann window. (b) Log-magnitude of transform.

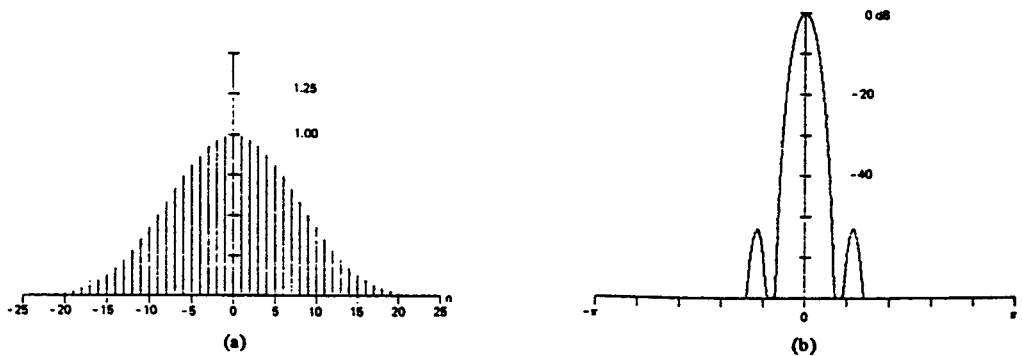


Fig. 29. (a) The de la Vallée-Poussin window. (b) Log-magnitude of transform.

tinuous, with a discontinuous first derivative at the boundary. It is similar to the Riesz and cosine lobe windows. The Riemann window is shown in Fig. 28.

3) *de la Vallée-Poussin (Jackson, Parzen) Window* [11]: The de la Vallée-Poussin window is a piecewise cubic curve obtained by self-convolving two triangles of half extent or four rectangles of one-fourth extent. It is defined as

$$w(n) = \begin{cases} 1.0 - 6 \left[ \frac{n}{N/2} \right]^2 \left[ 1.0 - \frac{|n|}{N/2} \right], & 0 \leq |n| \leq \frac{N}{4} \\ 2 \left[ 1.0 - \frac{|n|}{N/2} \right]^3, & \frac{N}{4} < |n| \leq \frac{N}{2} \end{cases} \quad (37)$$

The window is continuous up to its third derivative so that its sidelobes fall off like  $1/\omega^4$ . The window is shown in Fig. 29. Notice the trade off of main-lobe width for sidelobe level. Compare this with the rectangle and the triangle. It is a non-negative window by virtue of its self-convolution construction.

4) *Tukey Window* [13]: The Tukey window, often called the cosine-tapered window, is best imagined as a cosine lobe of width  $(\alpha/2)N$  convolved with a rectangle window of width  $(1.0 - \alpha/2)N$ . Of course the resultant transform is the product of the two corresponding transforms. The window represents an attempt to smoothly set the data to zero at the boundaries while not significantly reducing the processing gain of the windowed transform. The window evolves from the rectangle to the Hanning window as the parameter  $\alpha$  varies from zero to unity. The family of windows exhibits a confusing array of

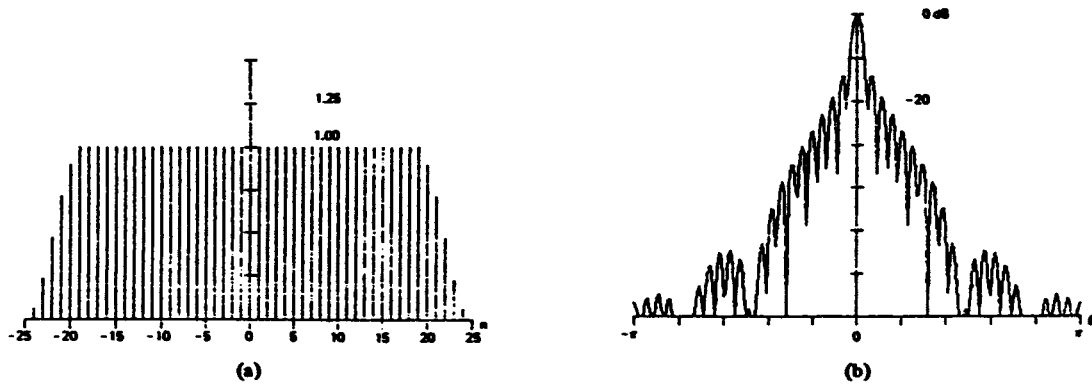


Fig. 30. (a) 25-percent cosine taper (Tukey) window. (b) Log-magnitude of transform.

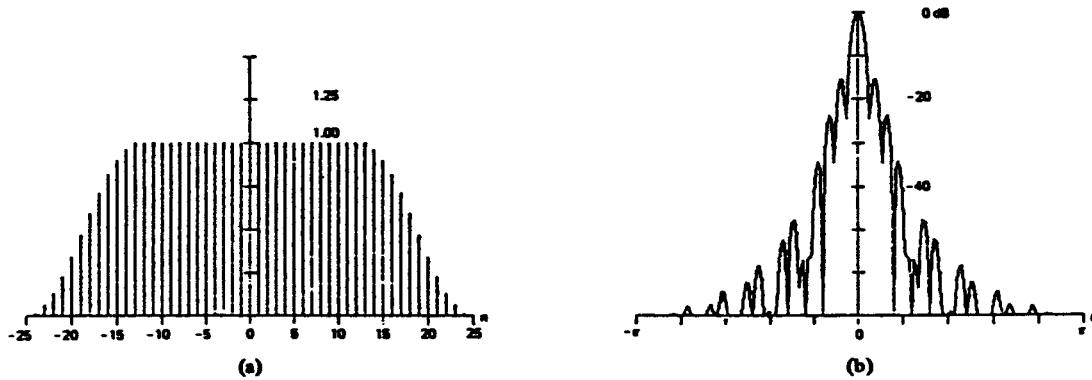


Fig. 31. (a) 50-percent cosine taper (Tukey) window. (b) Log-magnitude of transform.

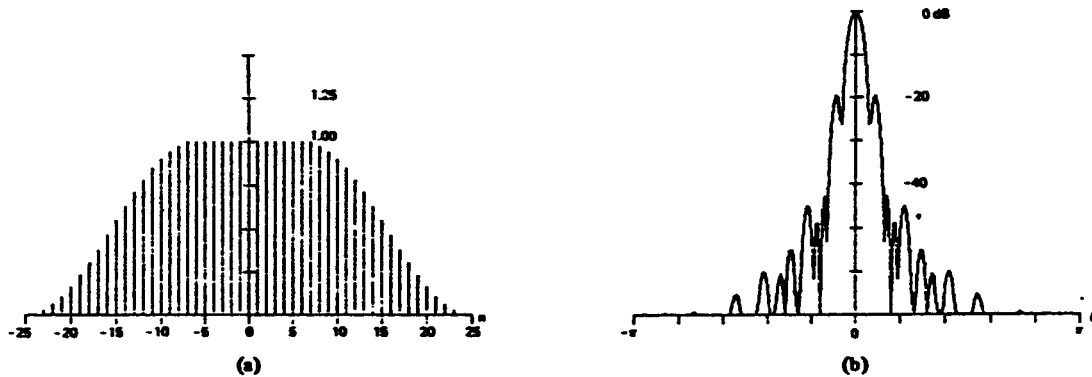


Fig. 32. (a) 75-percent cosine taper (Tukey) window. (b) Log-magnitude of transform.

sidelobe levels arising from the product of the two component transforms. The window is defined by

$$w(n) = \begin{cases} 1.0, & 0 < |n| < \frac{N}{2} \\ 0.5 \left[ 1.0 + \cos \left[ \pi \frac{n - \frac{N}{2}}{2(1 - \alpha) \frac{N}{2}} \right] \right], & \alpha \frac{N}{2} < |n| < \frac{N}{2} \end{cases} \quad (38)$$

The window is shown in Figs. 30-32 for values of  $\alpha$  equal to 0.25, 0.50, and 0.75, respectively.

5) *Bohman Window* [14]: The Bohman window is ob-

tained by the convolution of two half-duration cosine lobes (26a), thus its transform is the square of the cosine lobe's transform (see Fig. 16). In the time domain the window can be described as a product of a triangle window with a single cycle of a cosine with the same period and, then, a corrective term added to set the first derivative to zero at the boundary. Thus the second derivative is continuous, and the discontinuity resides in the third derivative. The transform falls off like  $1/\omega^4$ . The window is defined in the following and is shown in Fig. 33:

$$w(n) = \left[ 1.0 - \frac{|n|}{N/2} \right] \cos \left[ \pi \frac{|n|}{N/2} \right] + \frac{1}{\pi} \sin \left[ \pi \frac{|n|}{N/2} \right], \quad 0 < |n| < \frac{N}{2}. \quad (39)$$

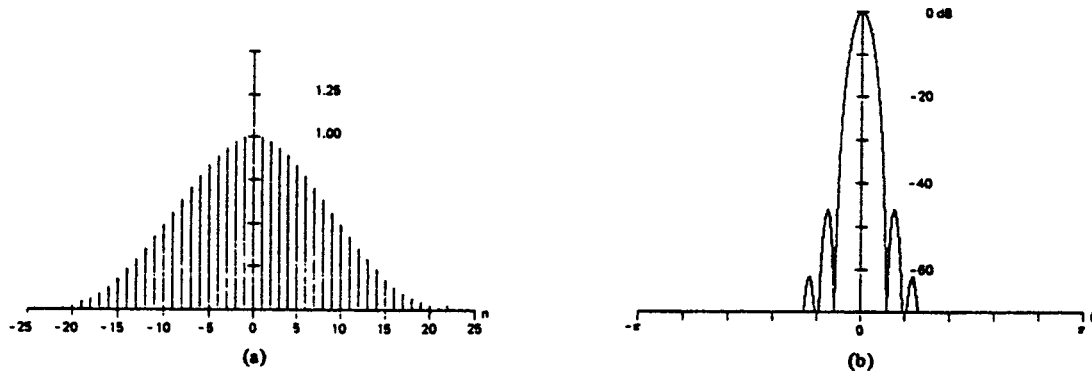
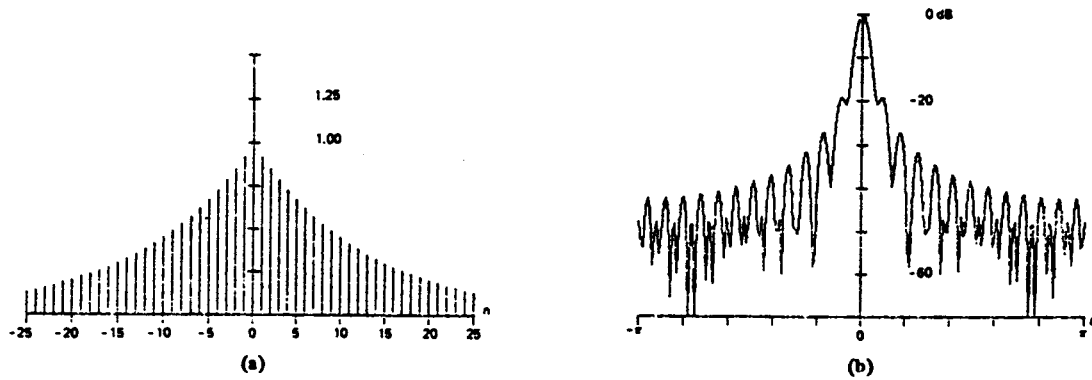
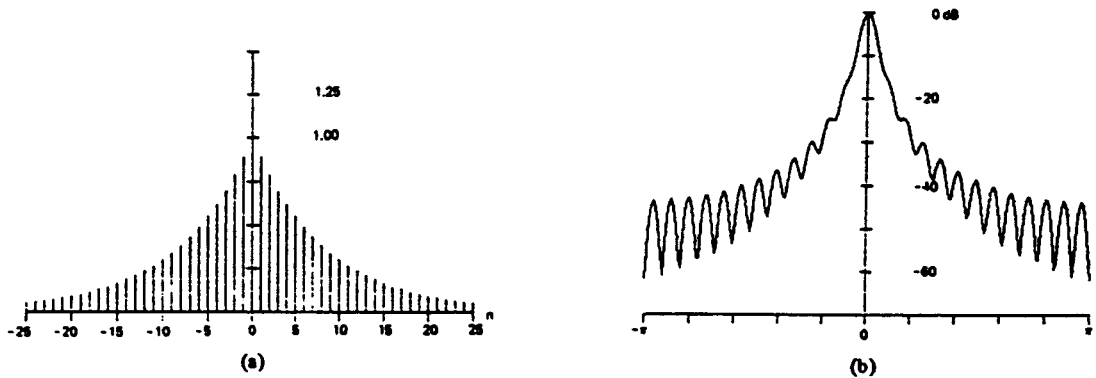


Fig. 33. (a) Bohman window. (b) Log-magnitude of transform.


 Fig. 34. (a) Poisson window. (b) Log-magnitude of transform ( $\alpha = 2.0$ ).

 Fig. 35. (a) Poisson window. (b) Log-magnitude of transform ( $\alpha = 3.0$ ).

6) *Poisson Window* [12]: The Poisson window is a two-sided exponential defined by

$$w(n) = \exp\left(-\alpha \frac{|n|}{N/2}\right), \quad 0 \leq |n| \leq \frac{N}{2}. \quad (40)$$

This is actually a family of windows parameterized on the variable  $\alpha$ . Since it exhibits a discontinuity at the boundaries, the transform can fall off no faster than  $1/\omega$ . The window is shown in Figs. 34–36 for values of  $\alpha$  equal to 2.0, 3.0, and 4.0, respectively. Notice as the discontinuity at the boundaries becomes smaller, the sidelobe structure merges into the asymptote. Also note the very wide main lobe; this will be

observed in Table I as a large equivalent noise bandwidth and as a large worst case processing loss.

7) *Hanning-Poisson Window*: The Hanning-Poisson window is constructed as the product of the Hanning and the Poisson windows. The family is defined by

$$w(n) = 0.5 \left[ 1.0 + \cos \left[ \pi \frac{n}{N/2} \right] \right] \exp\left(-\alpha \frac{|n|}{N/2}\right), \quad 0 \leq |n| \leq \frac{N}{2}. \quad (41)$$

This window is similar to the Poisson window. The rate of sidelobe falloff is determined by the discontinuity in the first

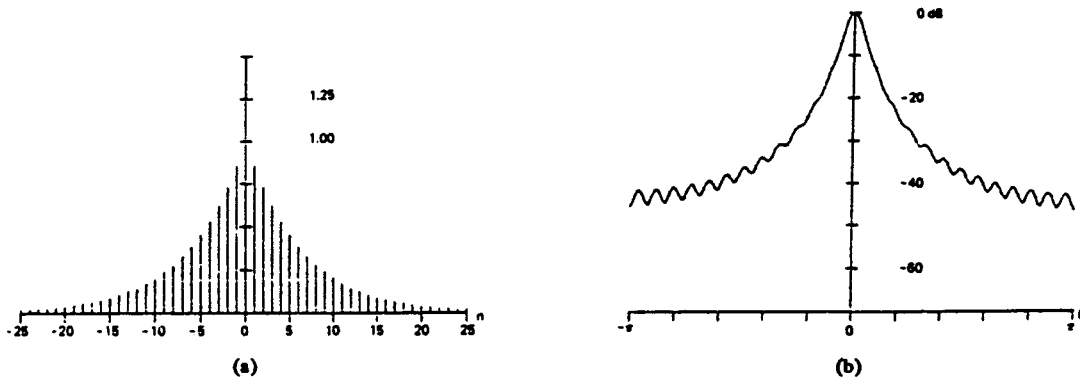


Fig. 36. (a) Poisson window. (b) Log-magnitude of transform ( $\alpha = 4.0$ ).

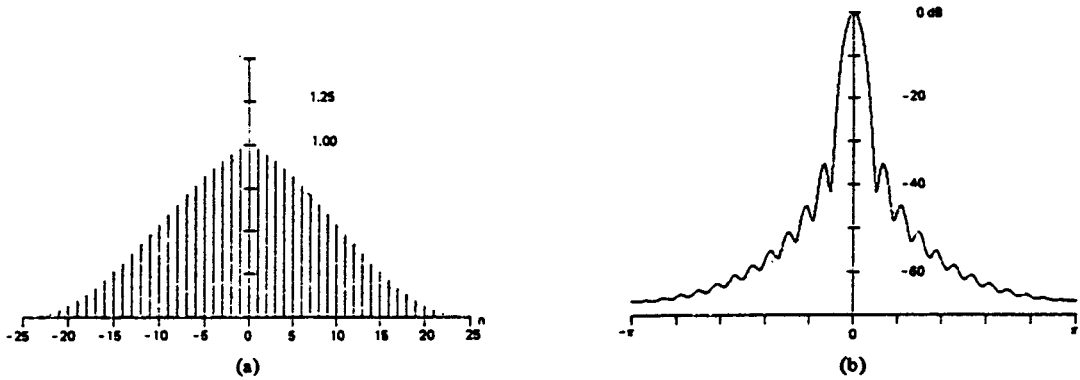


Fig. 37. (a) Hanning-Poisson window. (b) Log-magnitude of transform ( $\alpha = 0.5$ ).

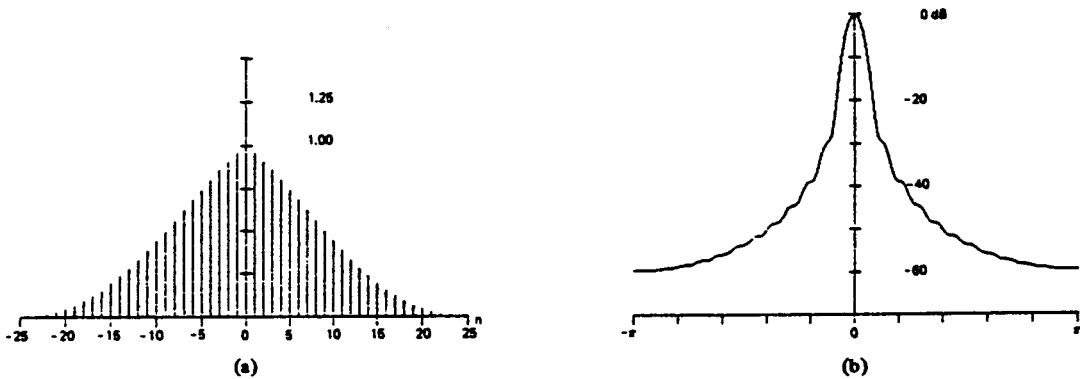


Fig. 38. (a) Hanning-Poisson window. (b) Log-magnitude of transform ( $\alpha = 1.0$ ).

derivative at the origin and is  $1/\omega^2$ . Notice as  $\alpha$  increases, forcing more of the exponential into the Hanning window, the zeros of the sidelobe structure disappear and the lobes merge into the asymptote. This window is shown in Figs. 37-39 for values of  $\alpha$  equal to 0.5, 1.0, and 2.0, respectively. Again note the very large main-lobe width.

8) *Cauchy (Abel, Poisson) Window* [15]: The Cauchy window is a family parameterized on  $\alpha$  and defined by

$$w(n) = \frac{1}{1.0 + \left[ \alpha \frac{n}{N/2} \right]^2}, \quad 0 \leq |n| \leq \frac{N}{2}. \quad (42)$$

The window is shown in Figs. 40-42 for values of  $\alpha$  equal to 3.0, 4.0, and 5.0, respectively. Note the transform of the

Cauchy window is a two-sided exponential (see Poisson windows), which when presented on a log-magnitude scale is essentially an isosceles triangle. This causes the window to exhibit a very wide main lobe and to have a large ENBW.

#### G. Gaussian or Weierstrass Window [15]

Windows are smooth positive functions with tall thin (i.e., concentrated) Fourier transforms. From the generalized uncertainty principle, we know we cannot simultaneously concentrate both a signal and its Fourier transform. If our measure of concentration is the mean-square time duration  $T$  and the mean-square bandwidth  $W$ , we know all functions satisfy the inequality of

$$TW \geq \frac{1}{4\pi} \quad (43)$$

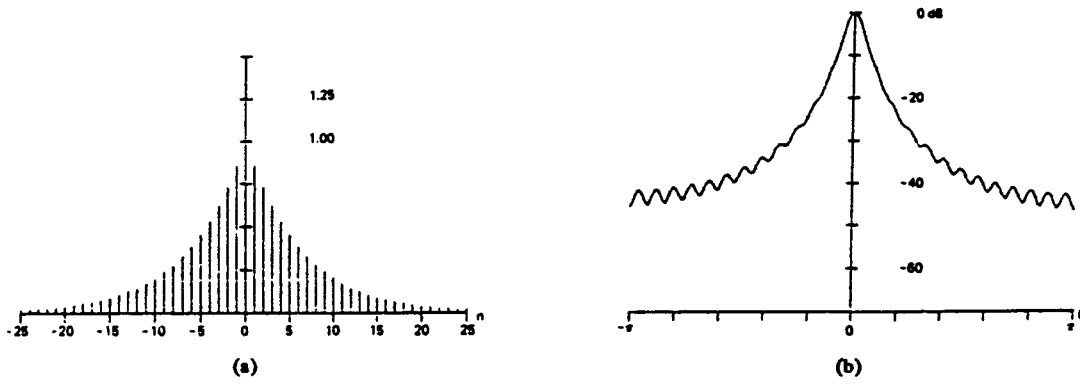


Fig. 36. (a) Poisson window. (b) Log-magnitude of transform ( $\alpha = 4.0$ ).

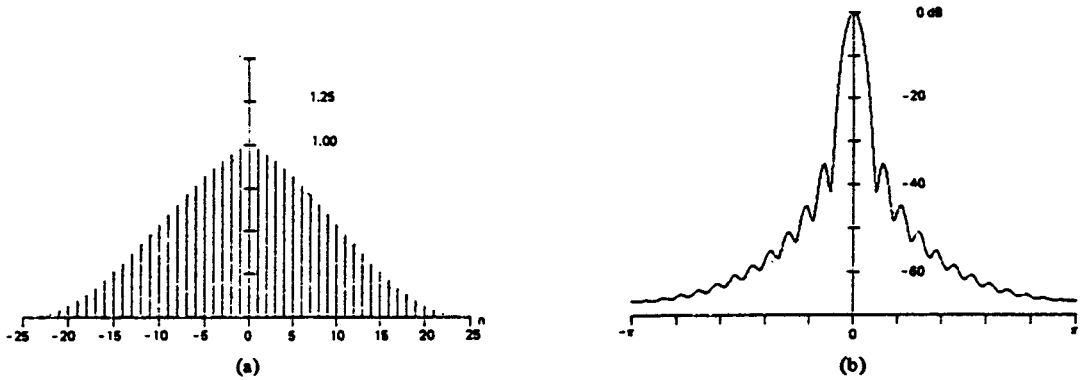


Fig. 37. (a) Hanning-Poisson window. (b) Log-magnitude of transform ( $\alpha = 0.5$ ).

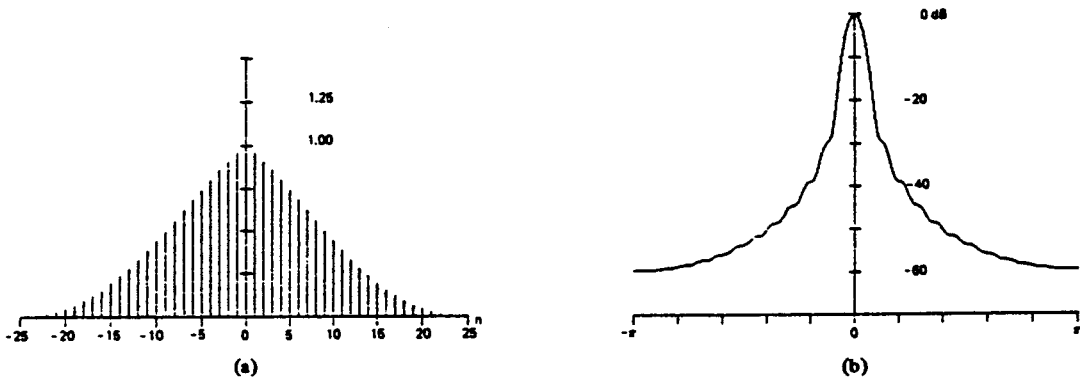


Fig. 38. (a) Hanning-Poisson window. (b) Log-magnitude of transform ( $\alpha = 1.0$ ).

derivative at the origin and is  $1/\omega^2$ . Notice as  $\alpha$  increases, forcing more of the exponential into the Hanning window, the zeros of the sidelobe structure disappear and the lobes merge into the asymptote. This window is shown in Figs. 37-39 for values of  $\alpha$  equal to 0.5, 1.0, and 2.0, respectively. Again note the very large main-lobe width.

8) *Cauchy (Abel, Poisson) Window* [15]: The Cauchy window is a family parameterized on  $\alpha$  and defined by

$$w(n) = \frac{1}{1.0 + \left[ \alpha \frac{n}{N/2} \right]^2}, \quad 0 \leq |n| \leq \frac{N}{2}. \quad (42)$$

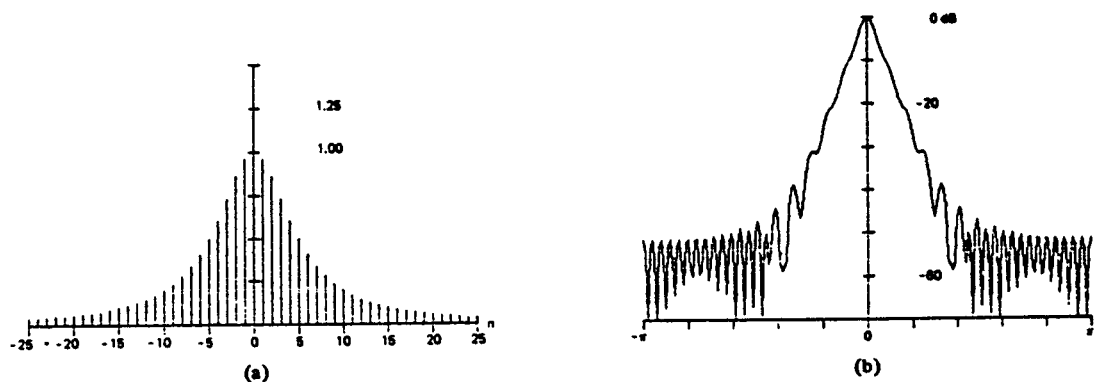
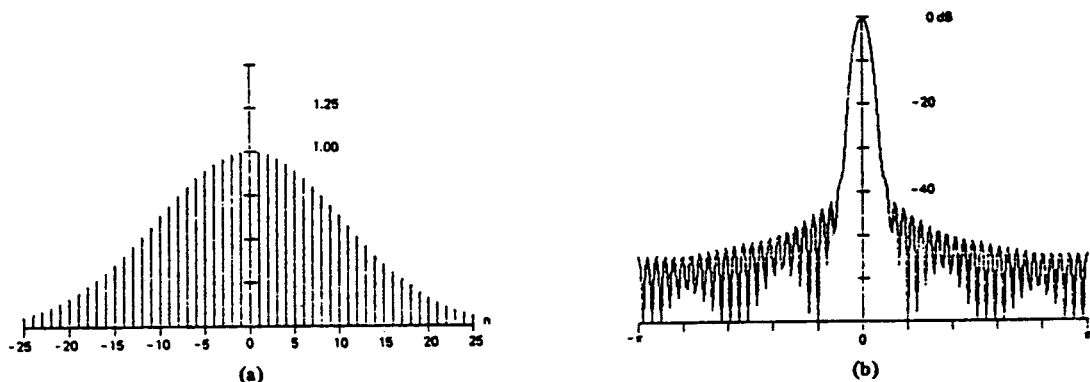
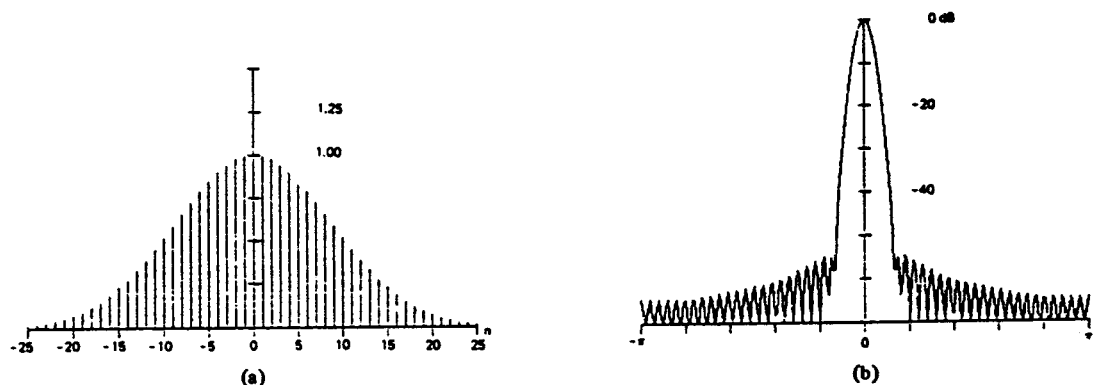
The window is shown in Figs. 40-42 for values of  $\alpha$  equal to 3.0, 4.0, and 5.0, respectively. Note the transform of the

Cauchy window is a two-sided exponential (see Poisson windows), which when presented on a log-magnitude scale is essentially an isosceles triangle. This causes the window to exhibit a very wide main lobe and to have a large ENBW.

#### G. Gaussian or Weierstrass Window [15]

Windows are smooth positive functions with tall thin (i.e., concentrated) Fourier transforms. From the generalized uncertainty principle, we know we cannot simultaneously concentrate both a signal and its Fourier transform. If our measure of concentration is the mean-square time duration  $T$  and the mean-square bandwidth  $W$ , we know all functions satisfy the inequality of

$$TW \geq \frac{1}{4\pi} \quad (43)$$

Fig. 42. (a) Cauchy window. (b) Log-magnitude of transform ( $a = 5.0$ ).Fig. 43. (a) Gaussian window. (b) Log-magnitude of transform ( $a = 2.5$ ).Fig. 44. (a) Gaussian window. (b) Log-magnitude of transform ( $a = 3.0$ ).

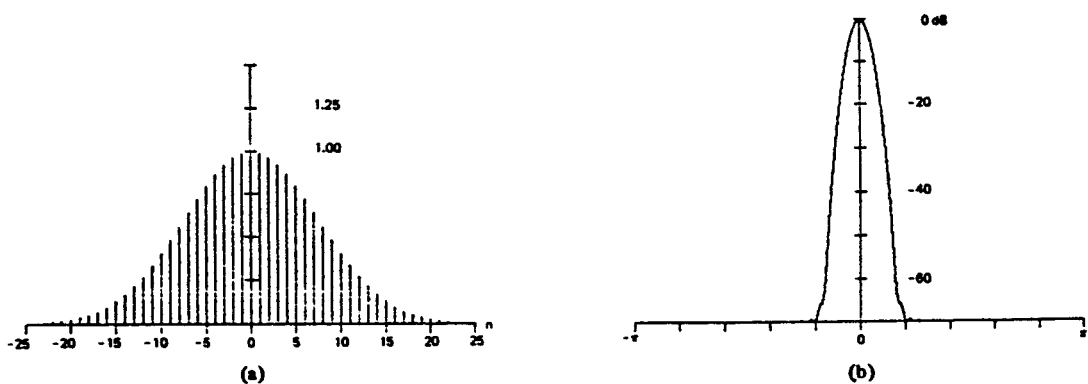
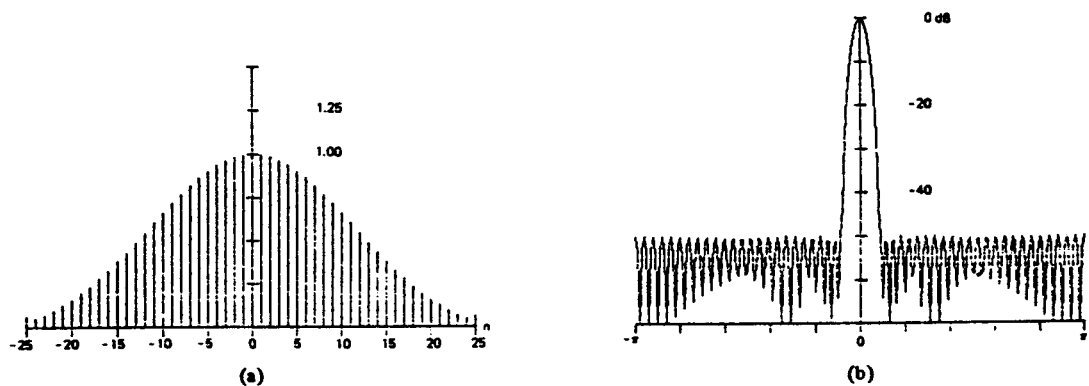
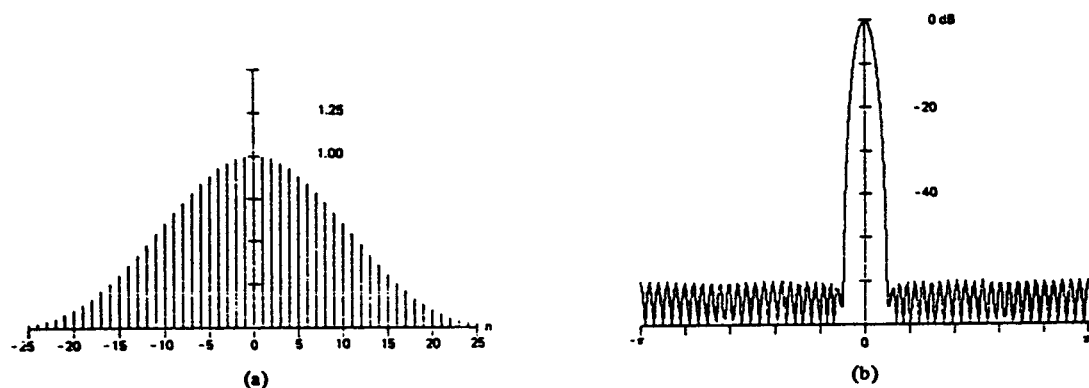
main lobe and decreased sidelobe levels. The window is presented in Figs. 43, 44, and 45 for values of  $\alpha$  equal to 2.5, 3.0, and 3.5, respectively. Note the rapid drop-off rate of sidelobe level in the exchange of sidelobe level for main-lobe width. The figures of merit for this window are listed in Table I

#### H. Dolph-Chebyshev Window [17]

Following the reasoning of the previous section, we seek a window which, for a known finite duration, in some sense exhibits a narrow bandwidth. We now take a lead from the antenna design people who have faced and solved a similar problem. The problem is to illuminate an antenna of finite

aperture to achieve a narrow main-lobe beam pattern while simultaneously restricting sidelobe response. (The antenna designer calls his weighting procedure *shading*.) The closed-form solution to the minimum main-lobe width for a given sidelobe level is the Dolph-Chebyshev window (shading). The continuous solution to the problem exhibits impulses at the boundaries which restricts continuous realizations to approximations (the Taylor approximation). The discrete or sampled window is not so restricted, and the solution can be implemented exactly.

The relation  $T_n(X) = \cos(n\theta)$  describes a mapping between the  $n$ th-order Chebyshev (algebraic) polynomial and the  $n$ th-order trigonometric polynomial. The Dolph-Chebyshev


 Fig. 45. (a) Gaussian window. (b) Log-magnitude of transform ( $\alpha = 3.5$ ).

 Fig. 46. (a) Dolph-Chebyshev window. (b) Log-magnitude of transform ( $\alpha = 2.5$ ).

 Fig. 47. (a) Dolph-Chebyshev window. (b) Log-magnitude of transform ( $\alpha = 3.0$ ).

window is defined with this mapping in the following equation, in terms of uniformly spaced samples of the window's Fourier transform,

$$W(k) = (-1)^k \frac{\cos \left[ N \cos^{-1} \left[ \beta \cos \left( \frac{k}{N} \right) \right] \right]}{\cosh [N \cosh^{-1}(\beta)]}, \quad 0 \leq |k| \leq N-1 \quad (45)$$

where

$$\beta = \cosh \left[ \frac{1}{N} \cosh^{-1}(10^\alpha) \right]$$

$$\cos^{-1}(X) = \begin{cases} \frac{\pi}{2} - \tan^{-1} [X/\sqrt{1.0 - X^2}], & |X| \leq 1.0 \\ \ln [X + \sqrt{X^2 - 1.0}], & |X| > 1.0. \end{cases}$$

To obtain the corresponding window time samples  $w(n)$ , we simply perform a DFT on the samples  $W(k)$  and then scale for unity peak amplitude. The parameter  $\alpha$  represents the log of the ratio of main-lobe level to sidelobe level. Thus a value of  $\alpha$  equal to 3.0 represents sidelobes 3.0 decades down from the main lobe, or sidelobes 60.0 dB below the main lobe. The  $(-1)^k$  alternates the sign of successive transform samples to reflect the shifted origin in the time domain. The window is

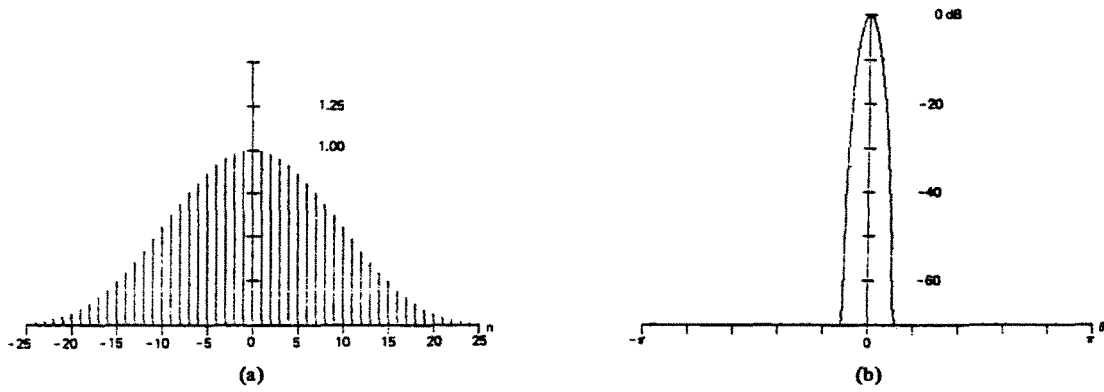


Fig. 48. (a) Dolph-Chebyshev window. (b) Log-magnitude of transform ( $\alpha = 3.5$ ).

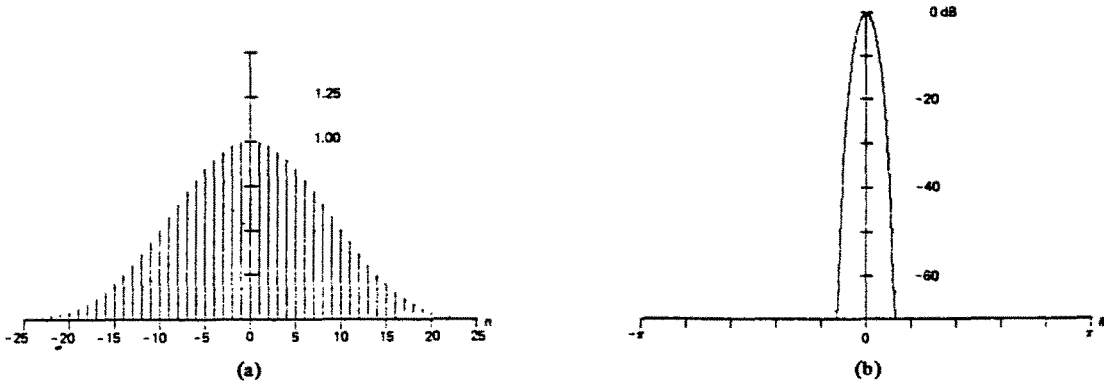


Fig. 49. (a) Dolph-Chebyshev window. (b) Log-magnitude of transform ( $\alpha = 4.0$ ).

presented in Figs. 46-49 for values of  $\alpha$  equal to 2.5, 3.0, 3.5, and 4.0, respectively. Note the uniformity of the sidelobe structure; almost sinusoidal! It is this uniform oscillation which is responsible for the impulses in the window.

#### I. Kaiser-Bessel Window [18]

Let us examine for a moment the optimality criteria of the last two sections. In Section V-G we sought the function with minimum time-bandwidth product. We know this to be the Gaussian. In Section V-H we sought the function with restricted time duration, which minimized the main-lobe width for a given sidelobe level. We now consider a similar problem. For a restricted energy, determine the function of restricted time duration  $T$  which maximizes the energy in the band of frequencies  $W$ . Slepian, Pollak, and Landau [19], [20] have determined this function as a family parameterized over the time-bandwidth product, the prolate-spheroidal wave functions of order zero. Kaiser has discovered a simple approximation to these functions in terms of the zero-order modified Bessel function of the first kind. The Kaiser-Bessel window is defined by

$$w(n) = \frac{I_0 \left[ \pi \alpha \sqrt{1.0 - \left( \frac{n}{N/2} \right)^2} \right]}{I_0[\pi \alpha]}, \quad 0 \leq |n| \leq \frac{N}{2} \quad (46a)$$

where

$$I_0(X) = \sum_{k=0}^{\infty} \frac{\left[ \left( \frac{X}{2} \right)^k \right]^2}{k!}.$$

The parameter  $\pi\alpha$  is half of the time-bandwidth product. The transform is approximately that of

$$W(\theta) \doteq \frac{N}{I_0(\pi\alpha)} \frac{\sinh \left[ \sqrt{\alpha^2 \pi^2 - (N\theta/2)^2} \right]}{\sqrt{\alpha^2 \pi^2 - (N\theta/2)^2}}. \quad (46b)$$

This window is presented in Figs. 50-53 for values of  $\alpha$  equal to 2.0, 2.5, 3.0, and 3.5, respectively. Note the trade off between sidelobe level and main-lobe width.

#### J. Barcilon-Temes Window [21]

We now examine the last criterion of optimality for a window. We have already described the Slepian, Pollak, and Landau criterion. Subject to the constraints of fixed energy and fixed duration, determine the function which maximizes the energy in the band of frequencies  $W$ . A related criterion, subject to the constraints of fixed area and fixed duration, is to determine the function which minimizes the energy (or the weighted energy) outside the band of frequencies  $W$ . This is a reasonable criterion since we recognize that the transform of a good window should minimize the energy it gathers from frequencies removed from its center frequency. Till now, we have been responding to this goal by maximizing the concentration of the transform at its main lobe.

A closed-form solution of the unweighted minimum-energy criterion has not been found. A solution defined as an expansion of prolate-spheroidal wave functions does exist and it is of the form shown in

$$H\left(\frac{\omega}{W}\right) = \sum_n \frac{\psi_{2n}(\pi\alpha, 0)}{1 - \lambda_{2n}} \psi_{2n}\left(\pi\alpha, \frac{\omega}{W}\right). \quad (47)$$



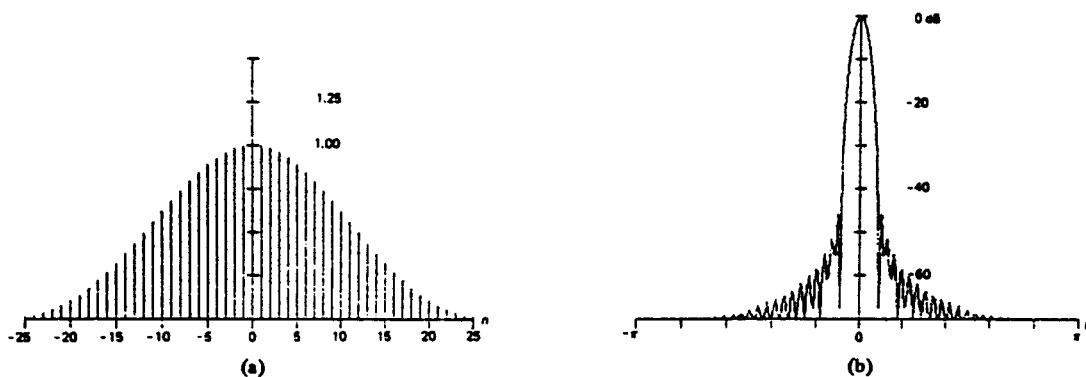


Fig. 50. (a) Kaiser-Bessel window. (b) Log-magnitude of transform ( $\alpha = 2.0$ ).

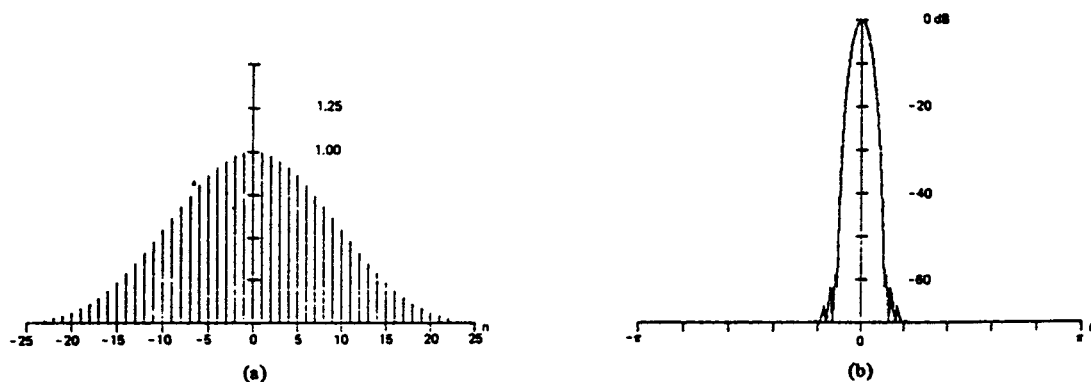


Fig. 51. (a) Kaiser-Bessel window. (b) Log-magnitude of transform ( $\alpha = 2.5$ ).

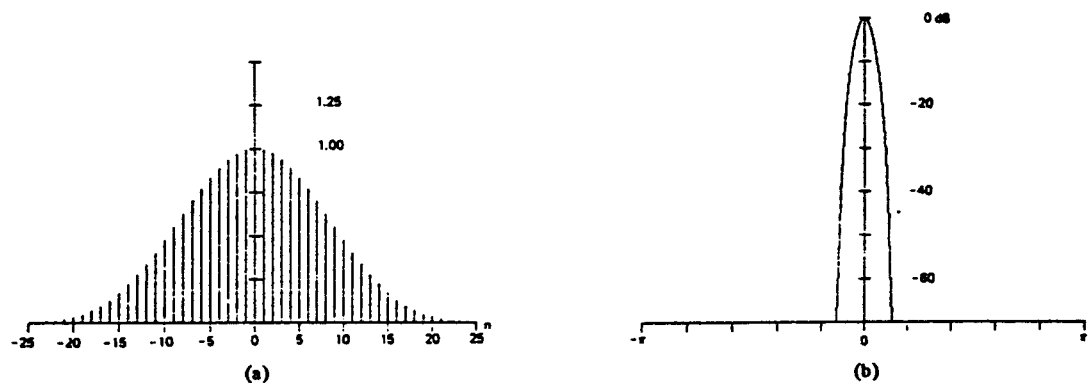


Fig. 52. (a) Kaiser-Bessel window. (b) Log-magnitude of transform ( $\alpha = 3.0$ ).

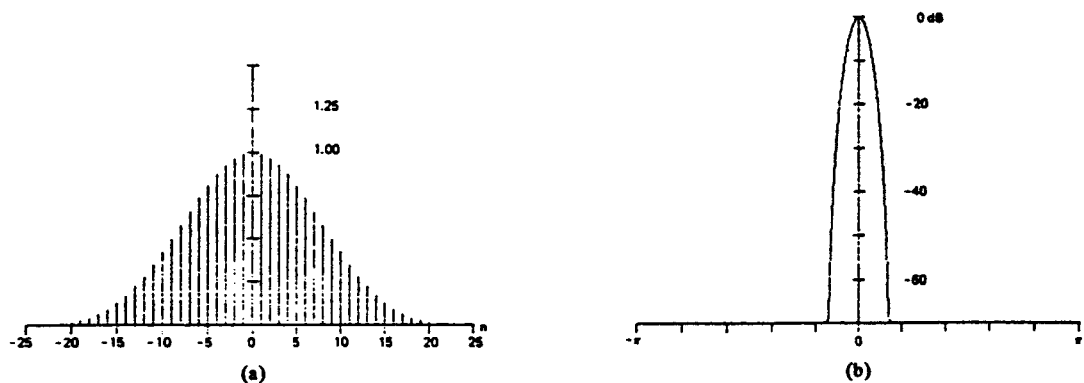


Fig. 53. (a) Kaiser-Bessel window. (b) Log-magnitude of transform ( $\alpha = 3.5$ ).

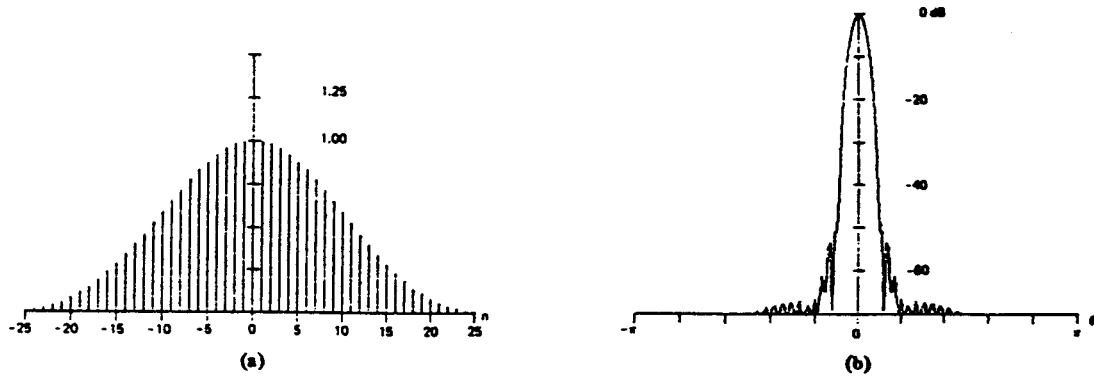


Fig. 54. (a) Barcion-Temes window. (b) Log-magnitude of transform ( $\alpha = 3.0$ ).

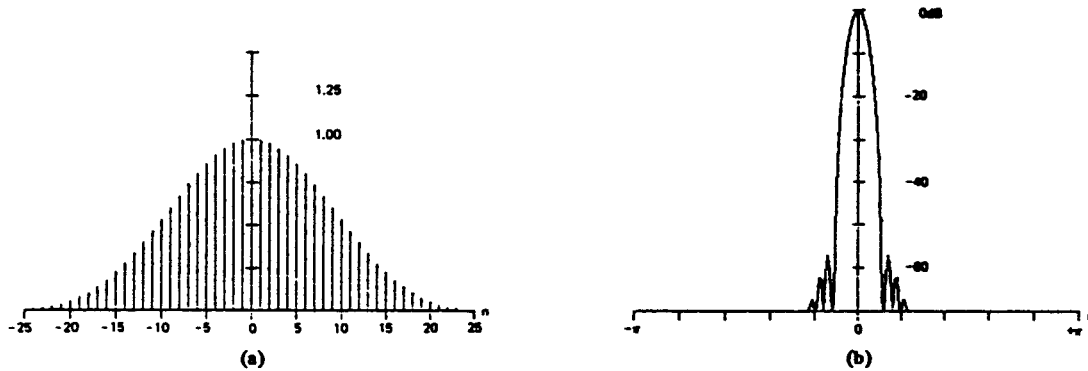


Fig. 55. (a) Barcion-Temes window. (b) Log-magnitude of transform ( $\alpha = 3.5$ ).

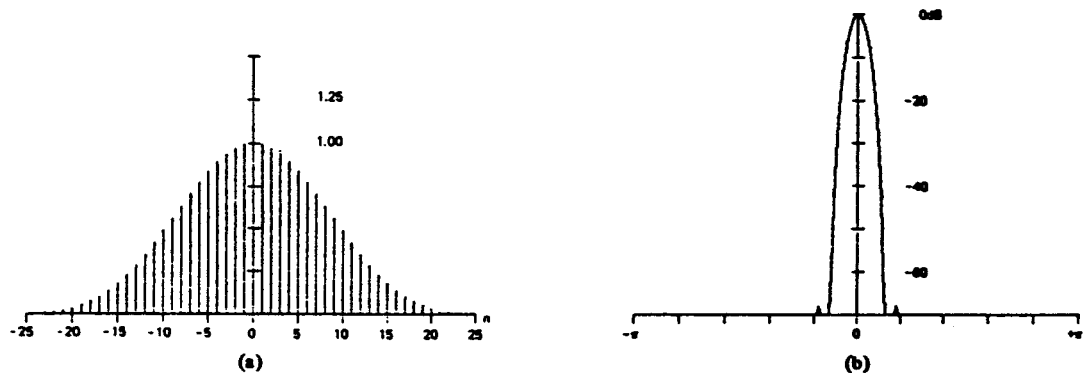


Fig. 56. (a) Barcion-Temes window. (b) Log-magnitude of transform ( $\alpha = 4.0$ ).

Here the  $\lambda_{2n}$  is the eigenvalue corresponding to the associated prolate-spheroidal wave function  $|\psi_{2n}(x, y)|$ , and the  $\pi\alpha$  is the selected half time-bandwidth product. The summation converges quite rapidly, and is often approximated by the first term or by the first two terms. The first term happens to be the solution of the Slepian, Pollak, and Landau problem, which we have already examined as the Kaiser-Bessel window.

A closed-form solution of a weighted minimum-energy criterion, presented in the following equation has been found by Barcion and Temes:

$$\text{Minimize } \int_{-\infty}^{\infty} |H(\omega)|^2 \frac{\omega}{\sqrt{\omega^2 - W^2}} d\omega. \quad (48) \quad \text{where}$$

This criterion is one which is a compromise between the Dolph-Chebyshev and the Kaiser-Bessel window criteria.

Like the Dolph-Chebyshev window, the Fourier transform is more easily defined, and the window time-samples are obtained by an inverse DFT and an appropriate scale factor. The transform samples are defined by

$$W(k) = (-1)^k \frac{A \cos \left[ \frac{y(k)}{C} \right] + B \left[ \frac{y(k)}{C} \sin \left[ \frac{y(k)}{C} \right] \right]}{[C + AB] \left[ \left[ \frac{y(k)}{C} \right]^2 + 1.0 \right]} \quad (49)$$

$$A = \sinh(C) = \sqrt{10^{2\alpha} - 1}$$

$$B = \cosh(C) = 10^\alpha$$

$$C = \cosh^{-1}(10^\alpha)$$

$$\beta = \cosh \left[ \frac{1}{N} C \right]$$

$$y(k) = N \cos^{-1} \left[ \beta \cos \left( \pi \frac{k}{N} \right) \right]$$

(See also (45).) This window is presented in Figs. 54–56 for values of  $\alpha$  equal to 3.0, 3.5, and 4.0, respectively. The main-lobe structure is practically indistinguishable from the Kaiser-Bessel main-lobe. The figures of merit listed on Table I suggest that for the same sidelobe level, this window does indeed reside between the Kaiser-Bessel and the Dolph-Chebyshev windows. It is interesting to examine Fig. 12 and note where this window is located with respect to the Kaiser-Bessel window; striking similarity in performance!

## VI. HARMONIC ANALYSIS

We now describe a simple experiment which dramatically demonstrates the influence a window exerts on the detection of a weak spectral line in the presence of a strong nearby line. If two spectral lines reside in DFT bins, the rectangle window allows each to be identified with no interaction. To demonstrate this, consider the signal composed of two frequencies  $10 f_s/N$  and  $16 f_s/N$  (corresponding to the tenth and the sixteenth DFT bins) and of amplitudes 1.0 and 0.01 (40.0 dB separation), respectively. The power spectrum of this signal obtained by a DFT is shown in Fig. 57 as a linear interpolation between the DFT output points.

We now modify the signal slightly so that the larger signal resides midway between two DFT bins; in particular, at  $10.5 f_s/N$ . The smaller signal still resides in the sixteenth bin. The power spectrum of this signal is shown in Fig. 58. We note that the sidelobe structure of the larger signal has completely swamped the main lobe of the smaller signal. In fact, we know (see Fig. 13) that the sidelobe amplitude of the rectangle window at 5.5 bins from the center is only 25 dB down from the peak. Thus the second signal (5.5 bins away) could not be detected because it was more than 26 dB down, and hence, hidden by the sidelobe. (The 26 dB comes from the 25-dB sidelobe level minus the 3.9-dB processing loss of the window plus 3.0 dB for a high confidence detection.) We also note the obvious asymmetry around the main lobe centered at 10.5 bins. This is due to the coherent addition of the sidelobe structures of the pair of kernels located at the plus and minus 10.5 bin positions. We are observing the self-leakage between the positive and the negative frequencies. Fig. 59 is the power spectrum of the signal pair, modified so that the large-amplitude signal resides at the 10.25-bin position. Note the change in asymmetry of the main-lobe and the reduction in the sidelobe level. We still can not observe the second signal located at bin position 16.0.

We now apply different windows to the two-tone signal to demonstrate the difference in second-tone detectability. For some of the windows, the poorer resolution occurs when the large signal is at 10.0 bins rather than at 10.5 bins. We will always present the window with the large signal at the location corresponding to worst-case resolution.

The first window we apply is the triangle window (see Fig. 60). The sidelobes have fallen by a factor of two over the rectangle windows' lobes (e.g., the -35-dB level has fallen to -70 dB). The sidelobes of the larger signal have fallen to approximately -43 dB at the second signal so that it is barely

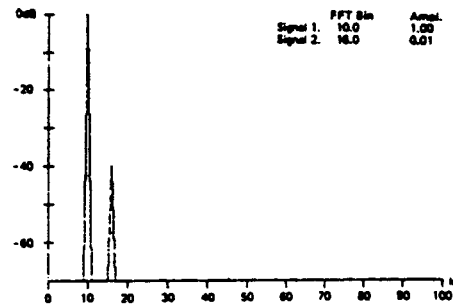


Fig. 57. Rectangle window.

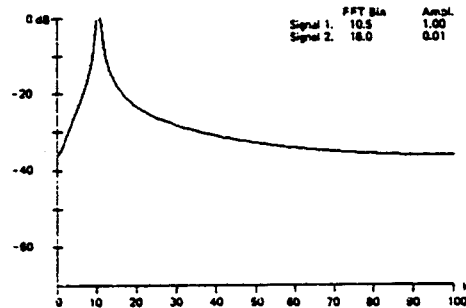


Fig. 58. Rectangle window.

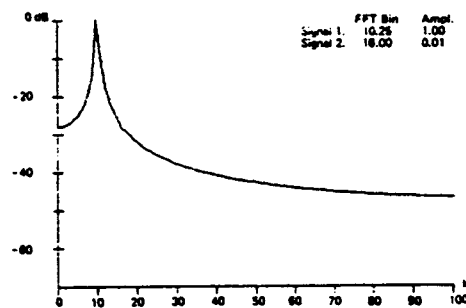


Fig. 59. Rectangle window.

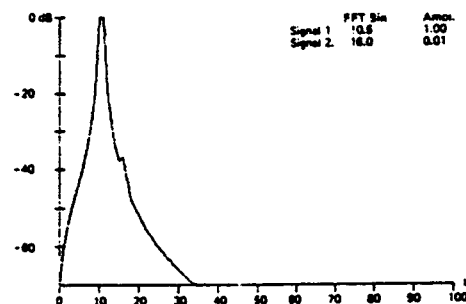


Fig. 60. Triangle window.

detectable. If there were any noise in the signal, the second tone would probably not have been detected.

The next windows we apply are the  $\cos^\alpha(x)$  family. For the cosine lobe,  $\alpha = 1.0$ , shown in Fig. 61 we observe a phase cancellation in the sidelobe of the large signal located at the small signal position. This cannot be considered a detection. We also see the spectral leakage of the main lobe over the frequency axis. Signals below this leakage level would not be detected. With  $\alpha = 2.0$  we have the Hanning window, which is

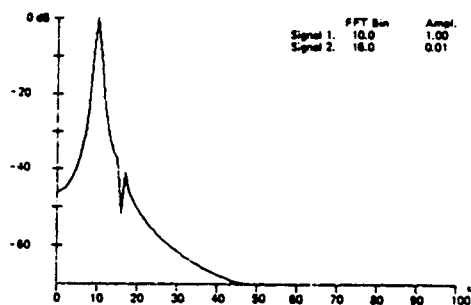
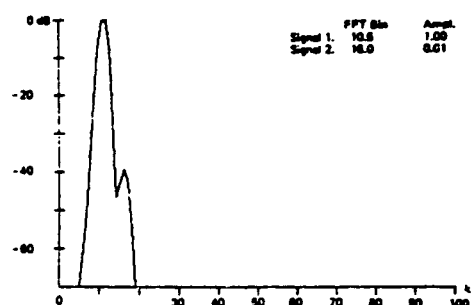
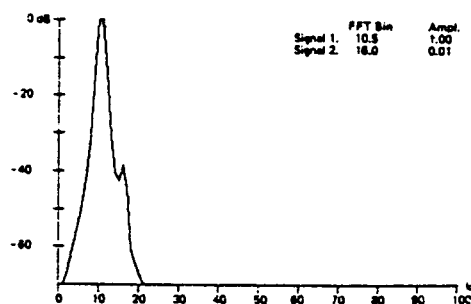
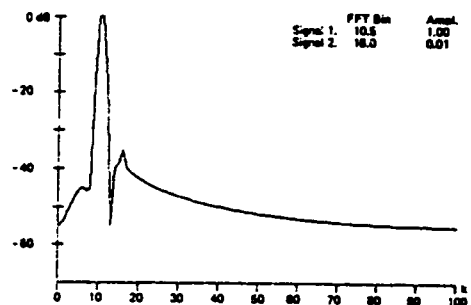
Fig. 61.  $\cos(\pi/N)$  window.Fig. 64.  $\cos^4(\pi/N)$  window.Fig. 62.  $\cos^3(\pi/N)$  window.

Fig. 65. Hamming window.

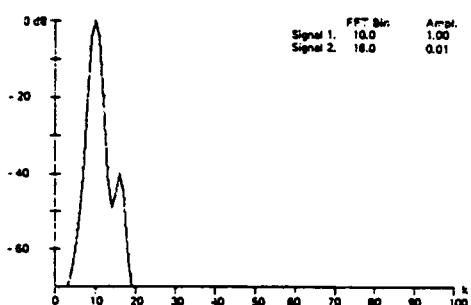
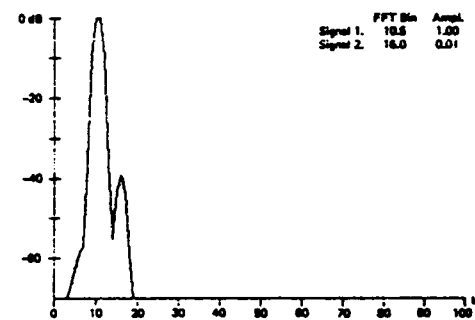
Fig. 63.  $\cos^3(\pi/N)$  window.

Fig. 66. Blackman window.

presented in Fig. 62. We detect the second signal and observe a 3.0-dB null between the two lobes. This is still a marginal detection. For the  $\cos^3(x)$  window presented in Fig. 63, we detect the second signal and observe a 9.0-dB null between the lobes. We also see the improved sidelobe response. Finally for the  $\cos^4(x)$  window presented in Fig. 64, we detect the second signal and observe a 7.0-dB null between the lobes. Here we witness the reduced return for the trade between sidelobe level and main-lobe width. In obtaining further reduction in sidelobe level we have caused the increased main-lobe width to encroach upon the second signal.

We next apply the Hamming window and present the result in Fig. 65. Here we observe the second signal some 35 dB down, approximately 3.0 dB over the sidelobe response of the large signal. Here, too, we observe the phase cancellation and the leakage between the positive and the negative frequency components. Signals more than 50 dB down would not be detected in the presence of the larger signal.

The Blackman window is applied next and we see the results in Fig. 66. The presence of the smaller amplitude kernel is now very apparent. There is a 17-dB null between the two signals. The artifact at the base of the large-signal kernel is

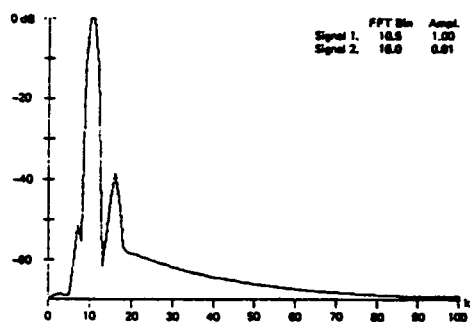


Fig. 67. Exact Blackman window.

the sidelobe structure of that kernel. Note the rapid rate of falloff of the sidelobe leakage has confined the artifacts to a small portion of the spectral line.

We next apply the exact Blackman coefficients and witness the results in Fig. 67. Again the second signal is well defined with a 24-dB null between the two kernels. The sidelobe structure of the larger kernel now extends over the entire spectral range. This leakage is not terribly severe as it is nearly

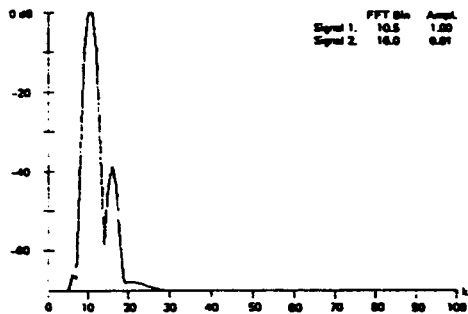


Fig. 68. Minimum 3-term Blackman-Harris window.

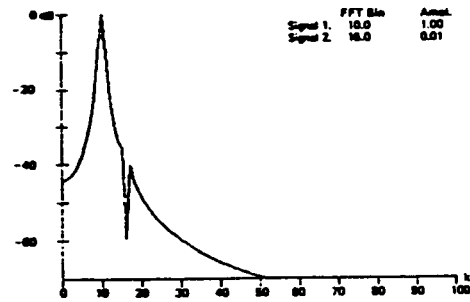


Fig. 71. Riesz window.

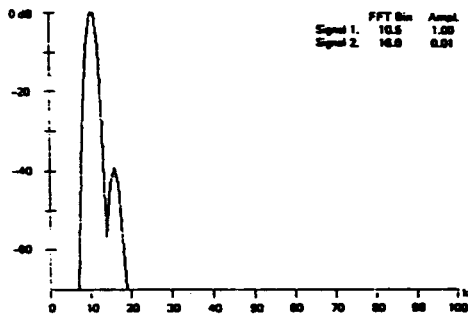


Fig. 69. 4-term Blackman-Harris window.

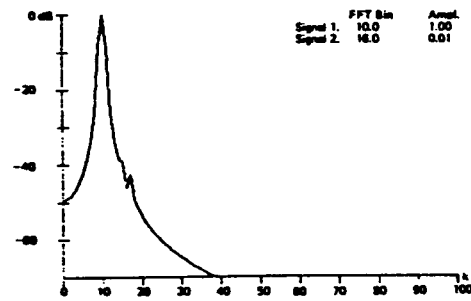


Fig. 72. Riemann window.

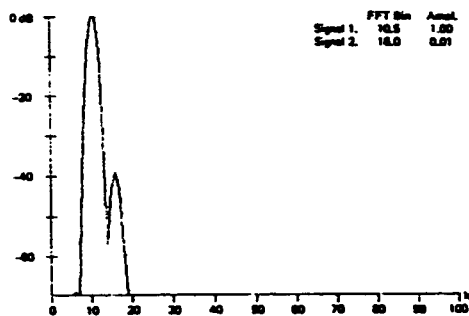


Fig. 70. 4-sample Kaiser-Bessel window.

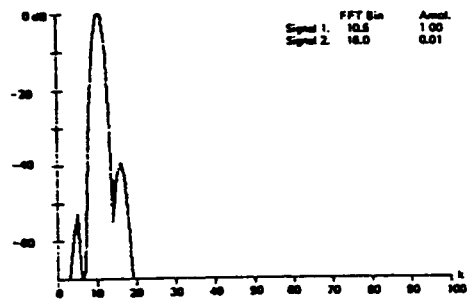


Fig. 73. de la Vallée-Poussin window.

60-dB down relative to the peak. There is another small artifact at 50-dB down on the low frequency side of the large kernel. This is definitely a single sidelobe of the large kernel. This artifact is essentially removed by the minimum 3-term Blackman-Harris window which we see in Fig. 68. The null between the two signal main lobes is slightly smaller, at approximately 20 dB.

Next the 4-term Blackman-Harris window is applied to the signal and we see the results in Fig. 69. The sidelobe structures are more than 70-dB down and as such are not observed on this scale. The two signal lobes are well defined with approximately a 19-dB null between them. Now we apply the 4-sample Kaiser-Bessel window to the signal and see the results in Fig. 70. We have essentially the same performance as with the 4-term Blackman-Harris window. The only observable difference on this scale is the small sidelobe artifact 68 dB down on the low frequency side of the large kernel. This group of Blackman-derived windows perform admirably well for their simplicity.

The Riesz window is the first of our constructed windows and is presented in Fig. 71. We have not detected the second signal but we do observe its affect as a 20.0-dB null due

to the phase cancellation of a sidelobe in the large signal's kernel.

The result of a Riemann window is presented in Fig. 72. Here, too, we have no detection of the second signal. We do have a small null due to phase cancellation at the second signal. We also have a large sidelobe response.

The next window, the de la Vallée-Poussin or the self-convolved triangle, is shown in Fig. 73. The second signal is easily found and the power spectrum exhibits a 16.0-dB null. An artifact of the window (its lower sidelobe) shows up, however, at the fifth DFT bin as a signal approximately 53.0 dB down. See Fig. 29.

The result of applying the Tukey family of windows is presented in Figs. 74-76. In Fig. 74 (the 25-percent taper) we see the lack of second-signal detection due to the high sidelobe structure of the dominant rectangle window. In Fig. 75 (the 50-percent taper) we observe a lack of second-signal detection, with the second signal actually filling in one of the nulls of the first signals' kernel. In Fig. 76 (the 76-percent taper) we witness a marginal detection in the still high sidelobes of the larger signal. This is still an unsatisfying window because of the artifacts.

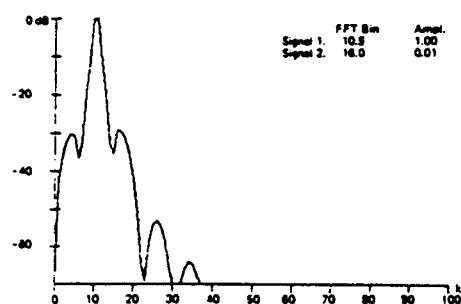


Fig. 74. Tukey (25-percent cosine taper) window.

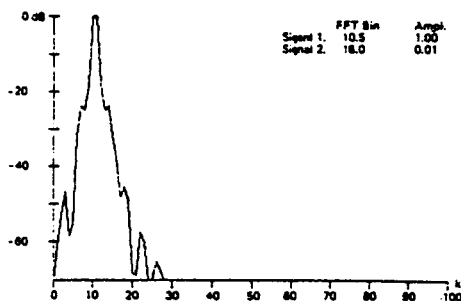


Fig. 75. Tukey (50-percent cosine taper) window.

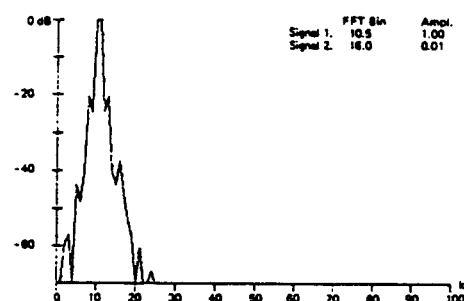


Fig. 76. Tukey (75-percent cosine taper) window.

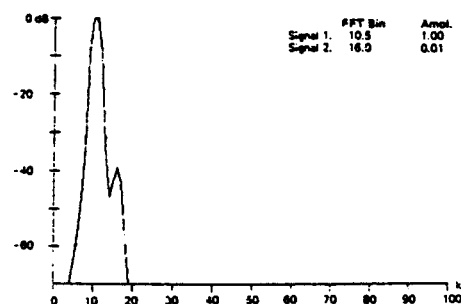
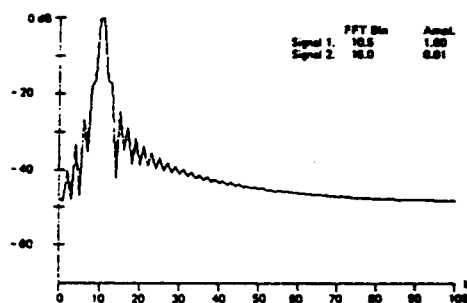
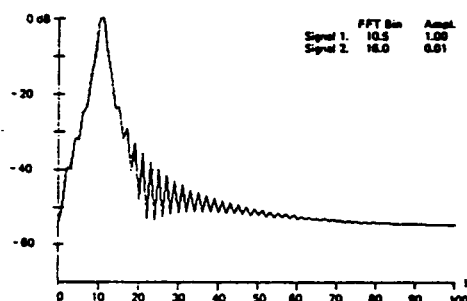
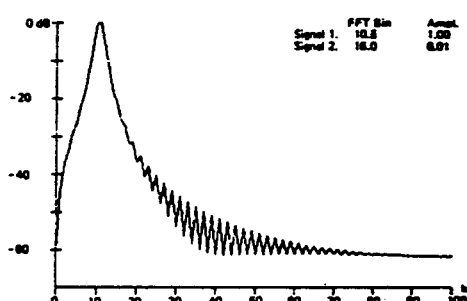


Fig. 77. Bohman window.

The Bohman construction window is applied and presented in Fig. 77. The second signal has been detected and the null between the two lobes is approximately 6.0 dB. This is not bad, but we can still do better. Note where the Bohman window resides in Fig. 12.

The result of applying the Poisson-window family is presented in Figs. 78–80. The second signal is not detected for any of the selected parameter values due to the high-sidelobe

Fig. 78. Poisson window ( $a = 2.0$ ).Fig. 79. Poisson window ( $a = 3.0$ ).Fig. 80. Poisson window ( $a = 4.0$ ).

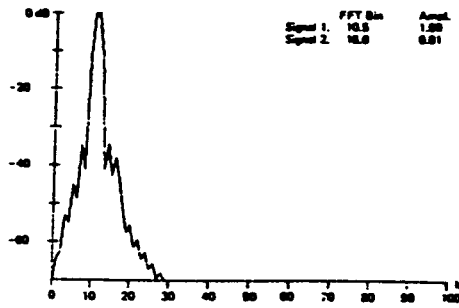
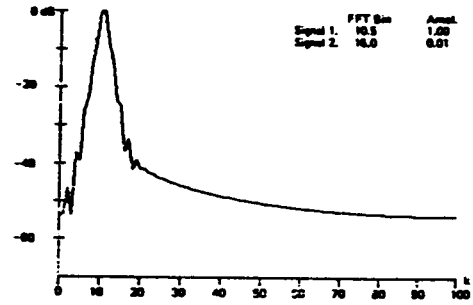
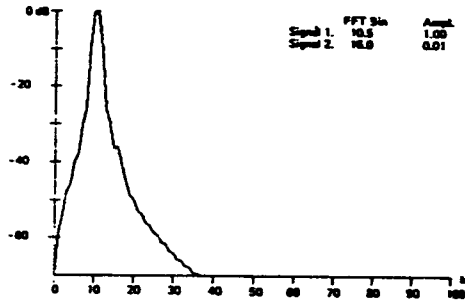
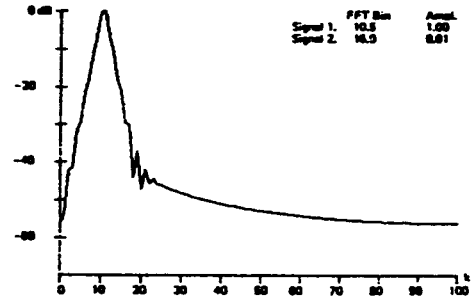
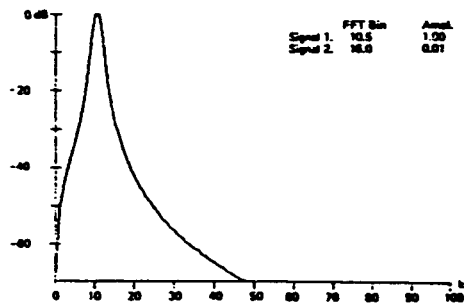
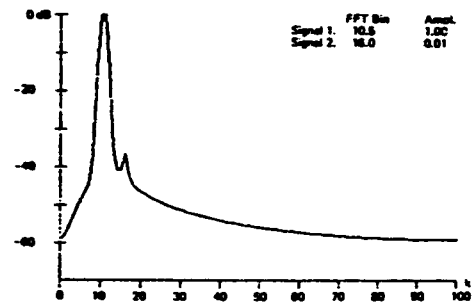
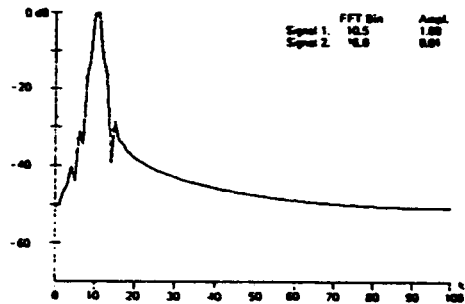
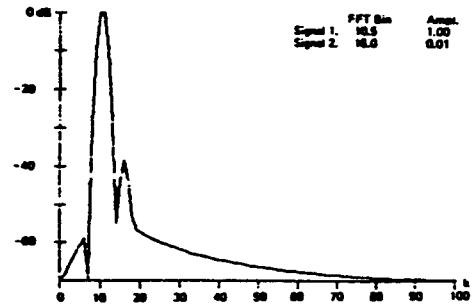
levels of the larger signal. We anticipated this poor performance in Table I by the large difference between the 3.0 dB and the ENBW.

The result of applying the Hanning-Poisson family of windows is presented in Figs. 81–83. Here, too, the second signal is either not detected in the presence of the high-sidelobe structure or the detection is bewildered by the artifacts.

The Cauchy-family windows have been applied and the results are presented in Figs. 84–86. Here too we have a lack of satisfactory detection of the second signal and the poor sidelobe response. This was predicted by the large difference between the 3.0 dB and the equivalent noise bandwidths as listed in Table I.

We now apply the Gaussian family of windows and present the results in Figs. 87–89. The second signal is detected in all three figures. We note as we further depress the sidelobe structure to enhance second-signal detection, the null deepens to approximately 16.0 dB and then becomes poorer as the main-lobe width increases and starts to overlap the lobe of the smaller signal.

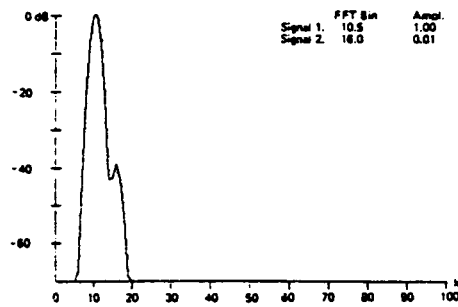
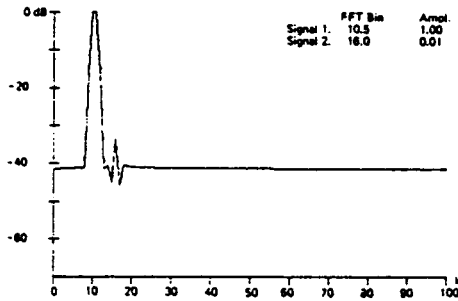
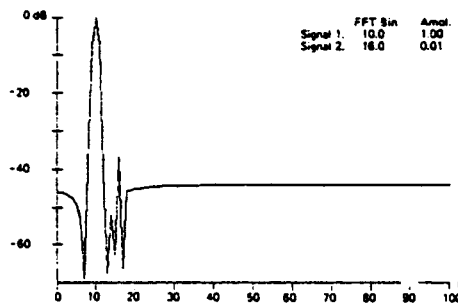
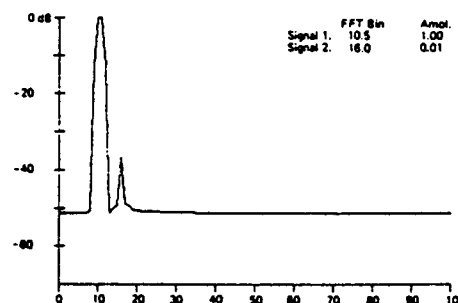
The Dolph-Chebyshev family of windows is presented in Figs. 90–94. We observe strong detection of the second signal


 Fig. 81. Hanning-Poisson window ( $a = 0.5$ ).

 Fig. 85. Cauchy window ( $a = 4.0$ ).

 Fig. 82. Hanning-Poisson window ( $a = 1.0$ ).

 Fig. 86. Cauchy window ( $a = 5.0$ ).

 Fig. 83. Hanning-Poisson window ( $a = 2.0$ ).

 Fig. 87. Gaussian window ( $a = 2.5$ ).

 Fig. 84. Cauchy window ( $a = 3.0$ ).

 Fig. 88. Gaussian window ( $a = 3.0$ ).

in all cases, but it is distressing to see the uniformly high side-lobe structure. Here, we again see the coherent addition of the sidelobes from the positive and negative frequency kernels. Notice that the smaller signal is not 40-dB down now. What we are seeing is the scalloping loss of the large signals' main-lobe being sampled off of the peak and being referenced as zero dB. Figs. 90 and 91 demonstrate the sensitivity of the sidelobe coherent addition to main-lobe position. In Fig. 90 the larger signal is at bin 10.5; in Fig. 91 it is at bin 10.0.

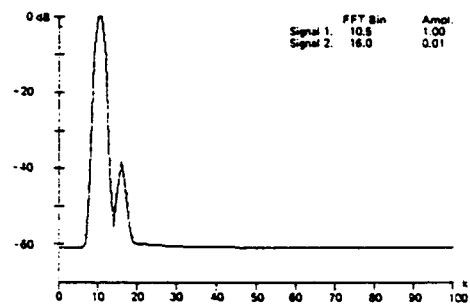
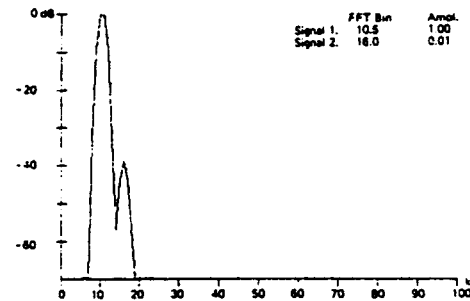
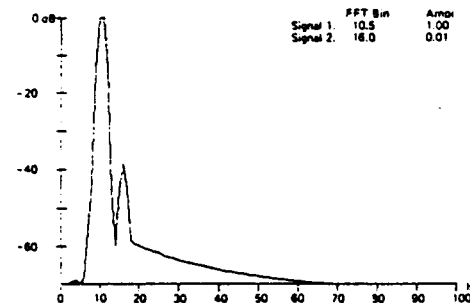
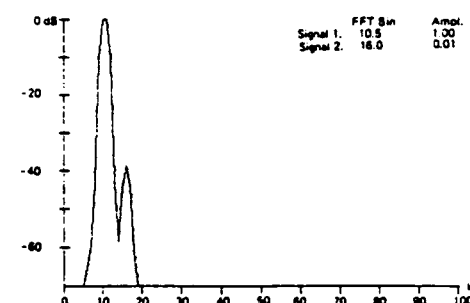
Note the difference in phase cancellation near the base of the large signal. Fig. 93, the 70-dB-sidelobe window, exhibits an 18-dB null between the two main lobes but the sidelobes have added constructively (along with the scalloping loss) to the -62.0-dB level. In Fig. 94, we see the 80-dB sidelobe window exhibited sidelobes below the 70-dB level and still managed to hold the null between the two lobes to approximately 18.0 dB.

The Kaiser-Bessel family is presented in Figs. 95-98. Here,


Fig. 89. Gaussian window ( $a = 3.5$ ).

Fig. 90. Dolph-Chebyshev window ( $a = 2.5$ ).

Fig. 91. Dolph-Chebyshev window ( $a = 2.5$ ).

Fig. 92. Dolph-Chebyshev window ( $a = 3.0$ ).

too, we have strong second-signal detection. Again, we see the effect of trading increased main-lobe width for decreased sidelobe level. The null between the two lobes reaches a maximum of 22.0 dB as the sidelobe structure falls and then becomes poorer with further sidelobe level improvement. Note that this window can maintain a 20.0-dB null between the two signal lobes and still hold the leakage to more than 70 dB down over the entire spectrum.

Figs. 99-101 present the performance of the Barcion-Temes window. Note the strong detection of the second signal.

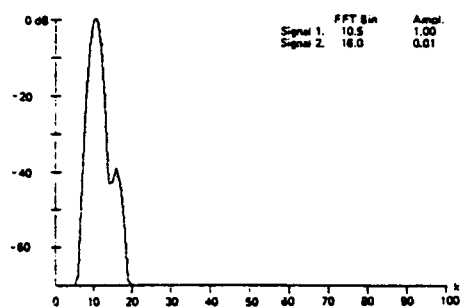
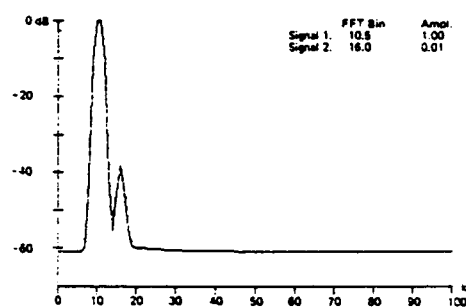
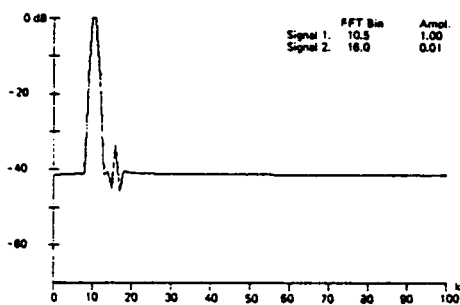
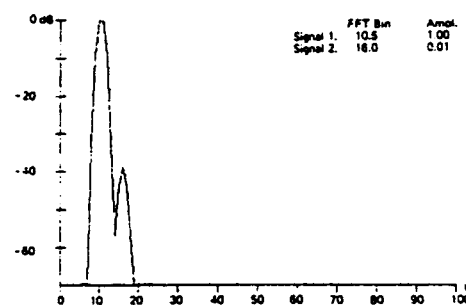
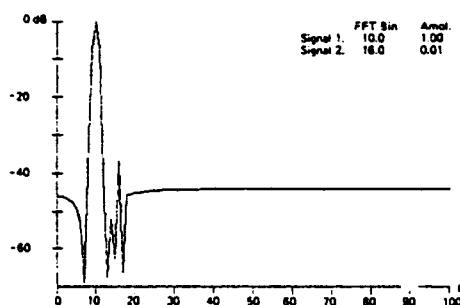
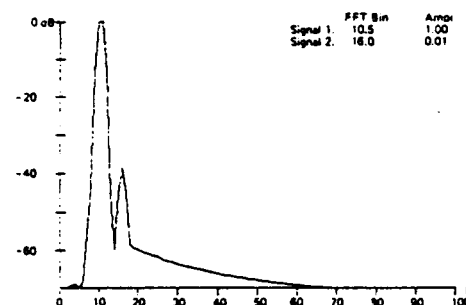
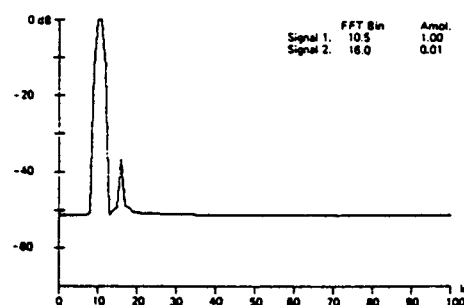
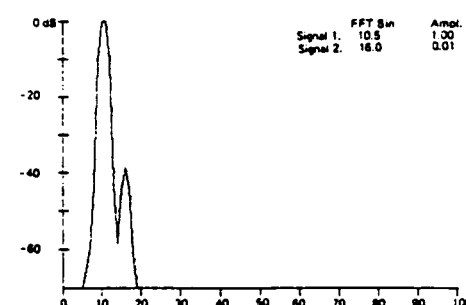

Fig. 93. Dolph-Chebyshev window ( $a = 3.5$ ).

Fig. 94. Dolph-Chebyshev window ( $a = 4.0$ ).

Fig. 95. Kaiser-Bessel window ( $a = 2.0$ ).

Fig. 96. Kaiser-Bessel window ( $a = 2.5$ ).

There are slight sidelobe artifacts. The window can maintain a 20.0-dB null between the two signal lobes. The performance of this window is slightly shy of that of the Kaiser-Bessel window, but the two are remarkably similar.

## VII. CONCLUSIONS

We have examined some classic windows and some windows which satisfy some criteria of optimality. In particular, we have described their effects on the problem of general har-



Fig. 89. Gaussian window ( $a = 3.5$ ).Fig. 93. Dolph-Chebyshev window ( $a = 3.5$ ).Fig. 90. Dolph-Chebyshev window ( $a = 2.5$ ).Fig. 94. Dolph-Chebyshev window ( $a = 4.0$ ).Fig. 91. Dolph-Chebyshev window ( $a = 2.5$ ).Fig. 95. Kaiser-Bessel window ( $a = 2.0$ ).Fig. 92. Dolph-Chebyshev window ( $a = 3.0$ ).Fig. 96. Kaiser-Bessel window ( $a = 2.5$ ).

too, we have strong second-signal detection. Again, we see the effect of trading increased main-lobe width for decreased sidelobe level. The null between the two lobes reaches a maximum of 22.0 dB as the sidelobe structure falls and then becomes poorer with further sidelobe level improvement. Note that this window can maintain a 20.0-dB null between the two signal lobes and still hold the leakage to more than 70 dB down over the entire spectrum.

Figs. 99-101 present the performance of the Barcion-Temes window. Note the strong detection of the second signal.

There are slight sidelobe artifacts. The window can maintain a 20.0-dB null between the two signal lobes. The performance of this window is slightly shy of that of the Kaiser-Bessel window, but the two are remarkably similar.

## VII. CONCLUSIONS

We have examined some classic windows and some windows which satisfy some criteria of optimality. In particular, we have described their effects on the problem of general har-

## APPENDIX

## THE EQUIVALENCE OF WINDOWING IN THE TIME DOMAIN TO CONVOLUTION IN THE FREQUENCY DOMAIN

Let

$$f(t) = \int_{-\infty}^{+\infty} F(\omega) \exp(-j\omega t) d\omega/2\pi$$

and

$$W(\omega) = \sum_{n=-N/2}^{+N/2} w(nT) \exp(+j\omega nT).$$

Then

$$F_w(\omega) = \sum_{n=-\infty}^{+\infty} w(nT) f(nT) \exp(+j\omega nT)$$

becomes

$$\begin{aligned} F_w(\omega) &= \sum_{n=-\infty}^{+\infty} w(nT) \int_{-\infty}^{+\infty} F(x) \exp(-jx nT) dx/2\pi \\ &\quad \cdot \exp(+j\omega nT) \\ &= \int_{-\infty}^{+\infty} F(x) \sum_{n=-\infty}^{+\infty} w(nT) \exp[+j(\omega - x)nT] dx/2\pi \\ &= \int_{-\infty}^{+\infty} F(x) \sum_{n=-N/2}^{+N/2} w(nT) \exp[+j(\omega - x)nT] dx/2\pi \\ &= \int_{-\infty}^{+\infty} F(x) W(\omega - x) dx/2\pi \end{aligned}$$

or

$$F_w(\omega) = F(\omega) * W(\omega).$$

## REFERENCES

- [1] C. W. Helstrom, *Statistical Theory of Signal Detection*, 2nd ed. New York: Pergamon Press, 1968, Ch. IV, 4, pp. 124-130.
- [2] J. W. Cooley, P. A. Lewis, and P. D. Welch, "The finite Fourier transform," *IEEE Trans. Audio Electroacoust.*, vol. AU-17, pp. 77-85, June 1969.
- [3] J. W. Wozencraft and I. M. Jacobs, *Principles of Communication Engineering*. New York: Wiley, 1965, ch. 4.3, pp. 223-228.

- [4] C. Lanczos, *Discourse on Fourier Series*. New York: Hafner Publishing Co., 1966, ch. 1, pp. 29-30.
- [5] P. D. Welch, "The use of fast Fourier transform for the estimation of power spectra: A method based on time averaging over short, modified periodograms," *IEEE Trans. Audio Electroacoust.*, vol. AU-15, pp. 70-73, June 1967.
- [6] J. R. Rice, *The Approximation of Functions*, Vol. I. Reading, MA: Addison-Wesley, 1964, ch. 5.3, pp. 124-131.
- [7] R. B. Blackman and J. W. Tukey, *The Measurement of Power Spectra*. New York: Dover, 1958, appendix B.5, pp. 95-100.
- [8] L. Fejer, "Untersuchungen über Fouriersche Reihen," *Mat. Ann.*, 58, pp. 501-569, 1904.
- [9] L. R. Rabiner, B. Gold, and C. A. McGonegal, "An approach to the approximation problem for nonrecursive digital filters," *IEEE Trans. Audio Electroacoust.*, vol. AU-18, pp. 83-106, June 1970.
- [10] F. J. Harris, "High-resolution spectral analysis with arbitrary spectral centers and adjustable spectral resolutions," *J. Comput. Elec. Eng.*, vol. 3, pp. 171-191, 1976.
- [11] E. Parzen, "Mathematical considerations in the estimation of spectra," *Technometrics*, vol. 3, no. 2, pp. 167-190, May 1961.
- [12] N. K. Bary, *A Treatise on Trigonometric Series*, Vol. I. New York: Macmillan, 1964, ch. I.53, pp. 149-150, ch. I.68, pp. 189-192.
- [13] J. W. Tukey, "An introduction to the calculations of numerical spectrum analysis," in *Spectral Analysis of Time Series*, B. Harris, Ed. New York: Wiley, 1967, pp. 25-46.
- [14] H. Bohman, "Approximate Fourier analysis of distribution functions," *Arkiv Föer Matematik*, vol. 4, 1960, pp. 99-157.
- [15] N. I. Akhiezer, *Theory of Approximation*. New York: Ungar, 1956, ch. IV.64, pp. 118-120.
- [16] L. E. Franks, *Signal Theory*. Englewood Cliffs, NJ: Prentice-Hall, 1969, ch. 6.1, pp. 136-137.
- [17] H. D. Helms, "Digital filters with equiripple or minimax responses," *IEEE Trans. Audio Electroacoust.*, vol. AU-19, pp. 87-94, Mar. 1971.
- [18] F. F. Kuo and J. F. Kaiser, *System Analysis by Digital Computer*. New York: Wiley, 1966, ch. 7, pp. 232-238.
- [19] D. Slepian and H. Pollak, "Prolate-spheroidal wave functions, Fourier analysis and uncertainty-I," *Bell Tel. Syst. J.*, vol. 40, pp. 43-64, Jan. 1961.
- [20] H. Landau and H. Pollak, "Prolate-spheroidal wave functions, Fourier analysis and uncertainty-II," *Bell Tel. Syst. J.*, vol. 40, pp. 65-84, Jan. 1961.
- [21] V. Barillon and G. Temes, "Optimum impulse response and the Van Der Maas function," *IEEE Trans. Circuit Theory*, vol. CT-19, pp. 336-342, July 1972.

## BIBLIOGRAPHY-ADDITIONAL GENERAL REFERENCES

- R. B. Blackman, *Data Smoothing and Prediction*. Reading, MA: Addison-Wesley, 1965.
- D. R. Brillinger, *Time Series Data Analysis and Theory*. New York: Holt, Rinehart, and Winston, 1975.
- D. Gingras, "Time series windows for improving discrete spectra estimation," Naval Undersea Research and Development Center, Rep. NUC TN-715, Apr. 1972.
- F. J. Harris, "Digital signal processing," Class notes, San Diego State Univ., 1971.
- G. M. Jenkins, "General considerations in the estimation of spectra," *Technometrics*, vol. 3, no. 2, pp. 133-166, May 1961.